1985

Combined translational-rotational jumps in solid (alpha)-CO and CO(,2)

Shang-Bin Liu
College of William & Mary - Arts & Sciences

INFORMATION TO USERS

This reproduction was made from a copy of a document sent to us for microfilming. While the most advanced technology has been used to photograph and reproduce this document, the quality of the reproduction is heavily dependent upon the quality of the material submitted.

The following explanation of techniques is provided to help clarify markings or notations which may appear on this reproduction.

1. The sign or "target" for pages apparently lacking from the document photographed is "Missing Page(s)". If it was possible to obtain the missing page(s) or section, they are spliced into the film along with adjacent pages. This may have necessitated cutting through an image and duplicating adjacent pages to assure complete continuity.

2. When an image on the film is obliterated with a round black mark, it is an indication of either blurred copy because of movement during exposure, duplicate copy, or copyrighted materials that should not have been filmed. For blurred pages, a good image of the page can be found in the adjacent frame. If copyrighted materials were deleted, a target note will appear listing the pages in the adjacent frame.

3. When a map, drawing or chart, etc., is part of the material being photographed, a definite method of "sectioning" the material has been followed. It is customary to begin filming at the upper left hand corner of a large sheet and to continue from left to right in equal sections with small overlaps. If necessary, sectioning is continued again — beginning below the first row and continuing on until complete.

4. For illustrations that cannot be satisfactorily reproduced by xerographic means, photographic prints can be purchased at additional cost and inserted into your xerographic copy. These prints are available upon request from the Dissertations Customer Services Department.

5. Some pages in any document may have indistinct print. In all cases the best available copy has been filmed.

University Microfilms International
300 N. Zeeb Road
Ann Arbor, MI 48106

Liu, Shang-Bin

COMBINED TRANSLATIONAL-ROTATIONAL JUMPS IN SOLID ALPHA-CARBON MONOXIDE AND CARBON DIOXIDE

The College of William and Mary in Virginia PH.D. 1985

PLEASE NOTE:

In all cases this material has been filmed in the best possible way from the available copy. Problems encountered with this document have been identified here with a check mark ___✓___.

1. Glossy photographs or pages _____
2. Colored illustrations, paper or print _____
3. Photographs with dark background _____
4. Illustrations are poor copy _____
5. Pages with black marks, not original copy _____
6. Print shows through as there is text on both sides of page _____
7. Indistinct, broken or small print on several pages ___✓___
8. Print exceeds margin requirements _____
9. Tightly bound copy with print lost in spine _____
10. Computer printout pages with indistinct print _____
11. Page(s) _____ lacking when material received, and not available from school or author.
12. Page(s) _____ seem to be missing in numbering only as text follows.
13. Two pages numbered _____. Text follows.
14. Curling and wrinkled pages _____
15. Other _____

COMBINED TRANSLATIONAL-ROTATIONAL JUMPS IN SOLID α-CO AND CO_2

A Dissertation

Presented to

The Faculty of the Department of Physics

The College of William and Mary in Virginia

In Partial Fulfillment

of the Requirements for the Degree of

Doctor of Philosophy

---

by

Shang-Bin Liu

August 1985

APPROVAL SHEET

This dissertation is submitted in partial fulfillment of

the requirements for the degree of

Doctor of Philosophy

Author

Approved, August 1985

Mark S. Conradi, Chairman

Roy L. Champion

Harlan E. Schone

William J. Kessler

Kenneth G. Potzinger

Gary C. Defotis, Chemistry Department

DEDICATED TO MY FAMILY

TABLE OF CONTENTS

ACKNOWLEDGMENTS

I would like to express my appreciation to my advisor Dr. Mark Conradi for his continuous guidance and encouragement throughout the course of the research, his influence in Physics and NMR, and especially his friendship. I would also like to thank the faculty of the Department of Physics for their instruction and hospitality during my years of graduate study. I am also indebted to the members of my examining committee for their careful reading and criticism of the manuscript. Special thanks are given to Dr. William Kossler and Dr. Harlan Schone for their valuable suggestions.

I express my gratitude to Donald Joyce and Paul Guss who helped in the computer related matters, to William Vulcan, Sylvia Stout, Dianne Fannin, Paula Spratley, and Edward Lawrence for their kindly assistance and directions. John Bensel, Norman Rainville, and Melvin Woods have helped in designing and machining part of the cryogenic apparatus and they are acknowledged.

I am also deeply grateful to my research collaborators, Philip Kuhns, Montee Doverspike, Terry Gullion, and Jeff Walton, for many detailed discussions, co-operations, and of course their friendship. And I thank Sue-Wuai Wei, Meng Chou Wu, Ye Zhou, and other fellow graduate students for their friendship, impressions and motivations.

Finally, I express my appreciation to my host-parents Mr. and Mrs. Thomas Moore and to my parents, who gave my family in Williamsburg

their love, encouragement, and attention that have been very important during our stay in the United States. And to my beloved wife Shyu-Li and our daughter Jia-Whei who shared in my hopes and frustrations, for their love, patience, and understanding, I cannot begin to express my gratitude. Any outcome of this research should be dedicated to all of them.

LIST OF TABLES

LIST OF FIGURES

ABSTRACT

Combined translational-rotational jumps in two orientationally ordered solids, α-CO and CO_2, have been measured using C^{13} NMR. In the Pa3 structure of these solids, a molecule which jumps to a neighboring (presumably vacant) site will reorient, due to the orientationally ordered structure.

The rates of translation and rotation have been measured independently by using different NMR techniques. The rotations were detected at high field (14.7 MHz) through the modulation of the chemical shift anisotropy; spin echoes and stimulated echoes were used. The translational jumps modulate the dipolar interactions and were studied at low fields (1.256 MHz) with line narrowing and Slichter-Ailion slow motion (T_{1D}) experiments. The rates of translations and rotations agree, indicating that they are two aspects of one combined motion.

The shift anisotropies of α-phase $C^{13}O$ and $C^{13}O_2$ were found to be 350 ± 15 ppm and 325 ± 15 ppm, respectively; both values are in good agreement with previous NMR measurements. The jump rates of the combined motion in both materials obey the thermally activated expression: $\omega_j = \tau_j^{-1} = \omega_0 \exp(-E_a/kT)$. The activation parameters are $E_a/k = 2100$ K and $\omega_0 = 2 \times 10^{14}$ s^{-1} for α-CO and $E_a/k = 6600$ K and $\omega_0 = 2 \times 10^{13}$ s^{-1} for CO_2. The activation energies of α-CO and CO_2 from this study agree by corresponding states analysis with that found previously for the same motion in N_2O. All three molecular solids belong to the family of solids composed of small, linear molecules with Pa3 crystal structure. Unusually high frequency prefactors (ω_0) are seen in all three solids and are not understood. The high prefactors are also shown to appear in other molecular solids such as benzene and ammonia.

COMBINED TRANSLATIONAL-ROTATIONAL JUMPS IN SOLID α-CO AND CO_2

Chapter I

INTRODUCTION

Nuclear magnetic resonance (NMR) has been a powerful tool for characterizing and measuring structures and motions in molecular solids. Enormous information can be obtained from chemical shifts, relaxation times, and other properties of the resonance signals. By way of example, the existence of overall molecular rotations, internal rotations, and hydrogen bonds have been inferred from NMR. In molecular solids, the orientational freedom increases as the crystal is heated up from low temperature. The gain in orientational freedom upon heating is often associated with a phase change (transition) causing the ordered solid to become disordered. In the orientationally disordered (plastic) crystals, the reorientational and the translational motions are all quite fast ($\tau_{rot} \simeq 1$ psec and $\tau_{trans} \simeq 0.1$ μsec); the rates of these motions as well as the detailed changes at the order-disorder transition can be investigated by NMR. In most of the ordered molecular solids, however, the translational motion is too slow to be detected by NMR and only the rotational motion can be studied. It is only after the developement of the slow motion techniques (Sli64, Ail71, Loo66, Jee67) that the translational diffusion in orientationally ordered molecular solids could be studied. Reported here are measurements of diffusional motion in two orientationally ordered solids, namely α-CO and CO_2, using C^{13} NMR.

The diatomic molecules N_2 and CO and triatomic molecules N_2O and CO_2 form a family of similar molecular solids (Tol80, Par78). N_2 and CO, and N_2O and CO_2 are isoelectronic pairs. All four molecules are linear with end-for-end symmetry (or nearly so). Both N_2 and CO_2 have zero electronic dipole moment and the end-for-end symmetry of the molecules (NN and OCO) is readily seen. Molecules CO and N_2O (NNO) both possess a small dipole moment. The dipole moments of CO and N_2O are so small that their orienting influence is negligible in the solids (Mel64); the atoms in these two molecules are approximately the same size and moreover the two bond lengths of N_2O are nearly equal. As listed in Table 1, all of the molecules have fairly large negative quadrupole moments (Sto66). It has been shown (Koh60, Nag60, Mel64) that the anisotropic molecular interactions in all four systems are the electrical quadrupole-quadrupole and the anisotropic parts of the molecular repulsion and dispersion (van der Waals attraction). The quadrupole moments of N_2O and CO_2 are larger than those of CO and N_2, and effectively prevent molecular reorientation in these solids. Hence, solids N_2O (Blu35) and CO_2 (Gia37) exist in only one phase each at all temperatures at equilibrium (zero) pressure. Solid N_2 and CO, on the other hand, crystallize in two stable phases (α and β) at equilibrium vapor pressure (Gia33, Sco76, Cla32).

The crystal structure of the low temperature solids α-N_2 and α-CO are the same as those of solids N_2O and CO_2. The solids are all primitive cubic in structure belonging to space group Pa3 (an orientationally ordered fcc lattice, identical with the fcc form of H_2); there has been considerable discussion (Par78) as to whether the

TABLE I

Molecular Properties of CO, N_2, CO_2, and N_2O

	CO	N_2	CO_2	N_2O
Molecular Weight (g/mole)	28.010	28.016	44.011	44.016
Triple Point Temperature (K)	68.09[a]	63.14[b]	216.56[c]	182.3[d]
α–β Transition Temperature (K)	61.55[a]	35.61[b]	-----	-----
Dipole Moment[e] ($\times 10^{18}$ esu.cm)	0.112	0	0	0.166
Quadrupole Moment[e] ($\times 10^{26}$ esu.cm^2)	-2.5	-1.52	-4.3	-3.0
Low Temperature Solid Structure	Pa3[f] (α-CO)	Pa3[g] (α-N_2)	Pa3[f]	Pa3[f]
β-phase[f] Structure	hcp	hcp	-----	-----

[a]Ref. Cla32, Lea62.
[b]Ref. Gia33, Din62.
[c]Ref. Gia37, New62.
[d]Ref. Blu35, Ata74.
[e]Ref. Sto66.
[f]Ref. Par78, Sme24.
[g]Ref. Sco76, Par78.

structure of α-N_2 is $Pa3$ or $P2_13$. The $P2_13$ structure is derived from the $Pa3$ structure by slightly displacing the molecular centers along the cube diagonal (i.e. the molecular axes). One expects from the similarities of molecular properties and crystal structures that these solids obey some kind of corresponding states relation (Tol80) just as the family of classical rare gas solids (Cha77, Hen72, Cow76).

The phase diagram of carbon monoxide is very similar to that of nitrogen. Solid N_2 is known to have a high pressure γ-phase (Swe55, Mil69, Sch70) which exists above 3.5 kbar at low temperature. For solid CO, no high pressure phase has been found (Ste57, Sch70, Rai71). At equilibrium vapor pressure, the phase transition temperature ($T_{\alpha\beta}$) of solid N_2 ($T_{\alpha\beta}$ = 35.5 K) is smaller than that of solid CO ($T_{\alpha\beta}$ = 61.55 K) due to the fact that the quadrupole moment of N_2 is smaller (Par78). Above $T_{\alpha\beta}$, the solid β-CO (61.55 < T < 68.1 K) is an orientationally disordered (rotor) crystal (Li81), likewise for β-N_2 (35.6 < T < 63.1 K) (Str62). The β-phase solids all have hcp crystal structures (Veg34, Jor64, Par78) with nearly ideal but slightly temperature dependent c/a ratio (c/a= 1.634 for CO and 1.633 for N_2) (Li81, Sco76). The occurrence of the close-packed lattice (hcp or fcc) is common among rotor (plastic) crystals (She79, Par78). Rapid molecular reorientations (on the order of $\simeq 10^{12}$ s^{-1}) in the β-CO (Li81) and β-N_2 (Sco76, Dov84) have been investigated. Translational diffusion in liquid (Fuk79) and β-CO (Fuk77) are also quite fast, but slower than the rotations.

Solid carbon dioxide is known (Gia37, New62) to melt at 216.56 K with a high vapor pressure (5.112 atms). Solid CO_2 exists in only

one phase at all temperatures under equilibrium vapor pressure, similar to solid N_2O (T_m = 182.4 K) (Cow76). No other phases of CO_2 have been found up to 10 kbar above 77 K (Ste57).

As mentioned above, the solid phases of α-N_2, α-CO, CO_2, and N_2O all have the same (Pa3) crystal structure. In a Pa3 structure, there are four molecules per unit cell and the lattice (fcc) is composed of four interpenetrating simple cubic sublattices. All molecules on any one sublattice are parallel or anti-parallel to each other, lying along one of the four body diagonals of the cube (Fig.1). A given molecule has 12 nearest neighbors, none belonging to the same sublattice as the given molecule. As a consequence, a molecular translational jump should be accompanied by a rotational jump. Specifically, if a given molecule jumps onto a previously vacant neighboring site, it will find itself on a new sublattice and will reorient accordingly through the tetrahedral angle (70.5^o or 109.5^o).

A particular kind of orientational disorder remains in α-CO and N_2O solids: head-tail disorder. Calorimetric studies found that both solids possess residual entropy $\Delta S \simeq k \ln 2$ per molecule at low temperature (Blu35, Cla32, Ata74). The molecules of CO and N_2O are nearly symmetric head for tail so the molecules are randomly oriented head for tail at high temperatures. It was further supposed that the molecular reorientation rate ω_r becomes vanishingly small at temperatures low enough to cause head-tail (dipolar) ordering of these barely asymmetric molecules. Dielectric measurements (Nar82) as well as an O^{17} NMR line width study (Bro84) found that the rates extrapolate to one mean reorientation in times of order one hour at temperatures well

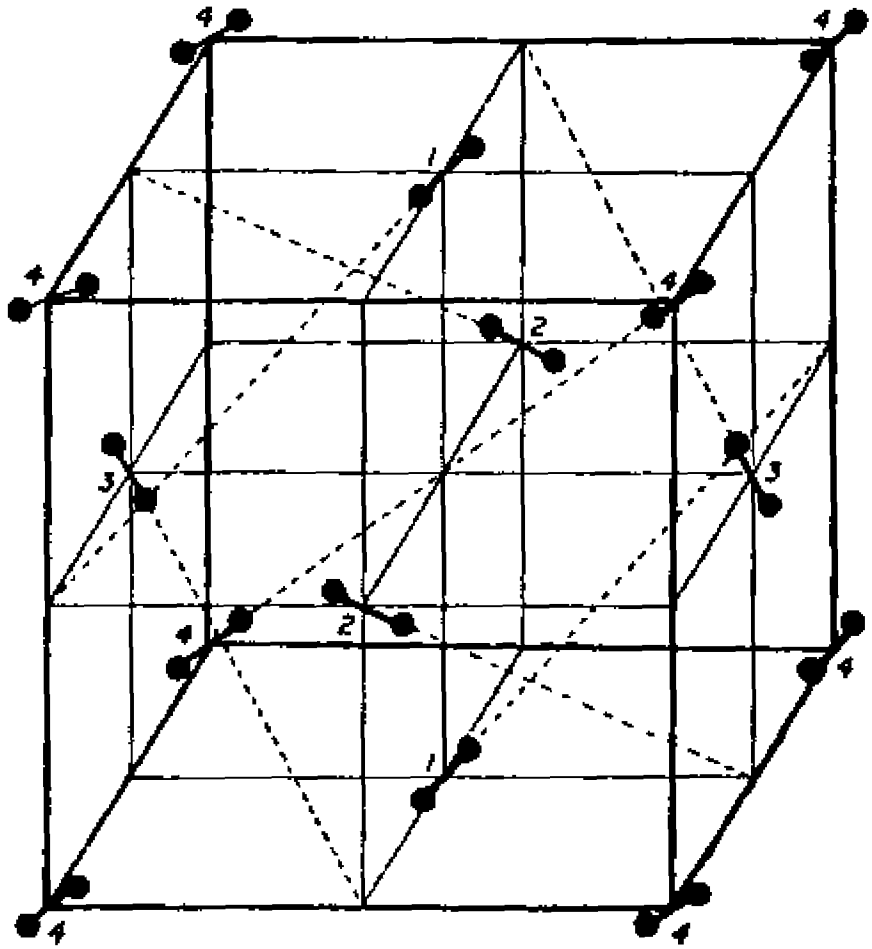

Figure 1: The Pa3 lattice structure (Par78) of α-CO, α-N_2, CO_2, and N_2O solids. The index numbers represent four interpenetrating simple cubic sub-lattices.

above the predicted dipolar ordering temperatures for both CO and N_2O solids. For α-CO and N_2O solids, the head-tail disorder characteristic of high temperature is locked in kinetically at low temperatures ($T < 17$ K for CO and $T < 112$ K for N_2O) (Nar82, Ata76). The molecule CO_2 is linear and symmetric about its geometric center. Thus the head-tail reorientations present in solid α-CO and N_2O are absent in CO_2 (or at least not detectable with dielectric techniques).

Combined translational-rotational jumps, the subject of this study, cannot be detected dielectrically in solid α-CO because much faster head-tail flips (Nar82) are occuring simultaneously. Solid CO_2 has zero dipole moment, so a dielectric study is not applicable. However, the combined jumps can be detected with NMR. The translational and rotational jump rates can be separately determined. The rotations were detected at high field by their effect on chemical shift anisotropy, as observed with lineshapes, spin echoes, and stimulated echoes. The translational jump rate was determined at low field through the modulation of the intermolecular dipole-dipole interactions, observed by line narrowing and the Slichter-Ailion slow motion experiment (T_{1D}) (Sli64, Ail71). It will be shown that the two jump rates separately measured in this way are essentially equal, as expected for the combined motion.

This technique was not applied to solid α-N_2 because the α-β transition of N_2 occurs at such a low temperature; the translational diffusion would likely be too slow to be detected. In the case of solid N_2O, N^{14} NMR measurements (Dov83) indicate that reorientation through an angle substantially different from 180° occurs in

solid N_2O. This reorientation cannot be the head-tail flips which occur in solid CO, but is probably due to the combined translational-rotational jumps. NMR measurements of translational diffusion in benzene (Gui85) and ammonia (Dov85) have also been investigated in this laboratory. Similar thermally activated diffusion motions with unusually high frequency prefactors were observed. These will be compared to the α-CO and CO_2 data of this report, and qualitative discussion as well as quantitative comparison will appear in Chapter V.

Chapter II

EXPERIMENTAL PROCEDURE

2.1 NMR SPECTROMETER

An NMR spectrometer is, to some extent, an analogy of a radio broadcasting system. Three major components are involved, namely a radio transmitter, an antenna (or transducer), and a radio receiver.

The block diagram of the computer-controlled pulsed NMR spectrometer is shown in Fig.2. A brief introduction to each of the major components of the spectrometer will be given in this section. This particular spectrometer is, in many aspects, similar to that presented in Ref. E1171 and more detailed discussion can be seen therein.

2.1.1 Magnet and Magnetic Field Control

A Varian V-4012A high impedance electromagnet was used. This water-cooled, iron-core magnet has a pair of poles (12 inches in diameter) seperated by a gap of about 1.75 inches. An air-cooled, current-regulated magnet power supply (V-2100B) furnishes power to the magnet. At maximum current (2 amps), the magnet generates a field strength of 15 kilo-gauss. In order to establish long term field stability, a home-made NMR frequency locker was used in conjunction with a Varian V-K3506 flux-stabilizer. The magnetic field controlling system is shown schematically in Fig.3.

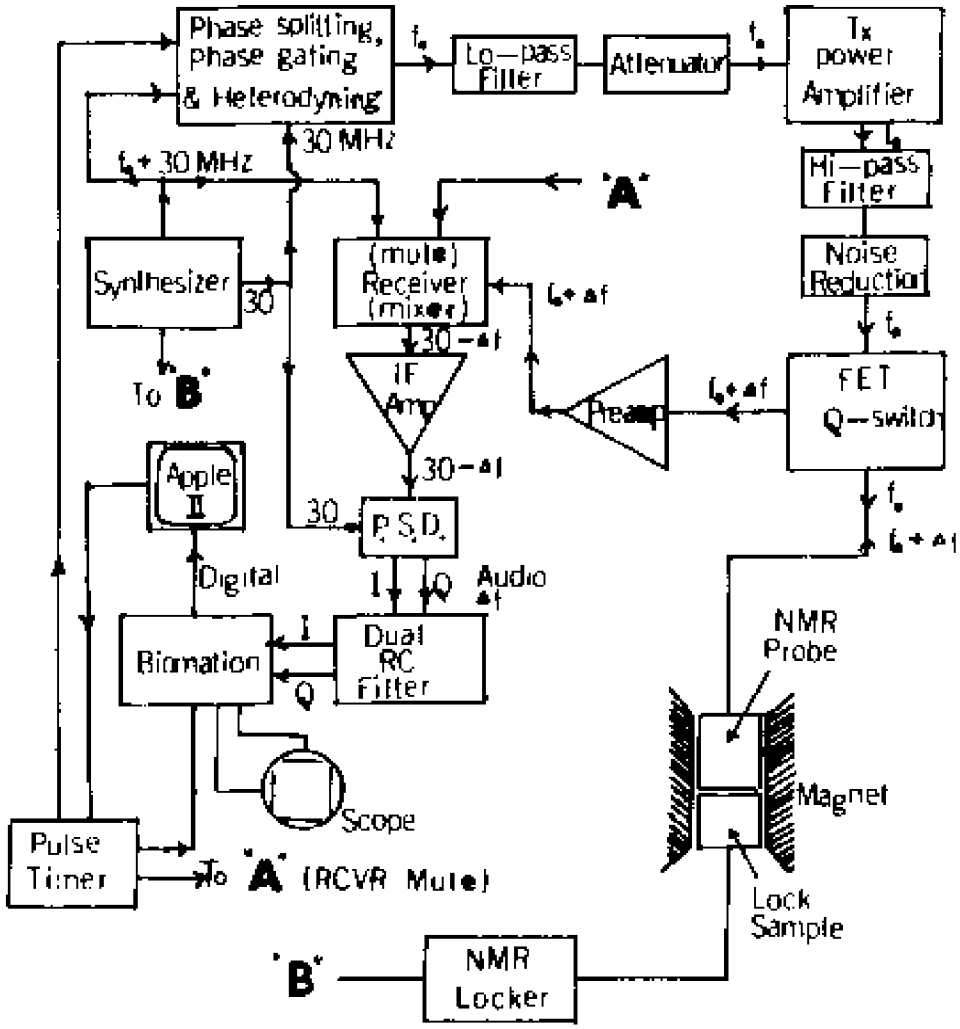

Figure 2: Block diagram of the computer-controlled pulsed NMR spectrometer used in the experiments.

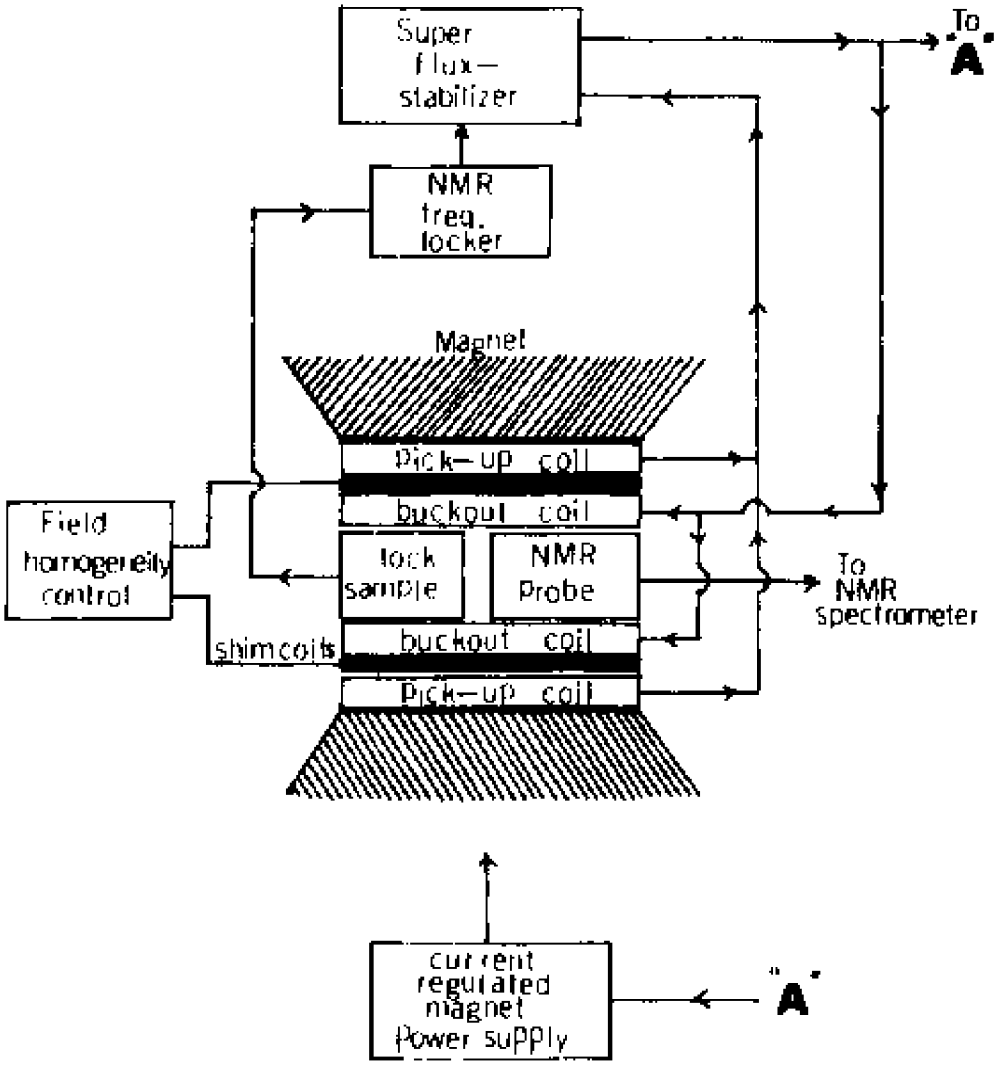

Figure 3: Schematic of the magnet and the magnetic field stability controlling system.

Long term field stability is established using the NMR frequency locker. The NMR frequency locker itself is a small NMR spectrometer. A detailed discussion of the NMR frequency locker has been presented before (Kuh83) and will not be given here. Basically, the NMR lock signal is obtained from the lock sample box placed near the center of the magnet (just outside the experimental dewar). The lock sample box usually contains a liquid sample of short T_1 (e.g. F^{19} in doped C_4F_6; $T_1 \approx 20$ ms) and a tank circuit tuned to the desired frequency. The NMR locker detects any small magnetic field change as a change in the time-averaged NMR signal from the lock sample; an error signal is fed back to the flux-stabilizer.

The flux-stabilizer has two pairs of Helmholtz coils (Fig.3), namely the pick-up coils and the buck out coils, placed at both sides of the magnet poles. The pick-up coils and the buck out coils are parts of a negative feedback loop which cancels (or removes) small fluctuations of the magnetic field. Part of the feedback signal from the stabilizer is also sent to the magnet power supply. In short, the flux-stabilizer served to provide short term field stability (that is it senses $d\Phi/dt$ and thus cannot provide long-term stability).

A pair of shim coils (Fig.3) connected to the field homogeneity control unit served to improve field homogeneity if desired. Magnetic field inhomogeneity produces field gradients which result in the broadening of the NMR line. The shim coils and the field homogeneity control unit essentially produce a reverse gradient, cancelling the field gradient of the magnet itself.

2.1.2 Probe and Matching Network

The NMR probe consists of a NMR coil in a tank circuit with a matching network to the transmitter and the receiver. The major roles of the probe are: first, it delivers transmitter power (in the form of oscillating magnetic field H_1) to the sample under study; secondly, it picks up the NMR signal from the sample (precessing magnetization) and sends it to the receiver.

Since a typical transmitter output signal is in the hundreds of volts range, and the receiver on the other hand is designed to receive and amplify signals in the microvolt range, one must isolate the transmitter and the receiver from each other to prevent the receiver from being overloaded or destroyed. That is, one isolates the receiver when the transmitter is on and vice versa. This is so called " duplexing". The single coil duplexing scheme has been used in this study due to the limited physical space in our low temperature apparatus and also due to its simplicity. The other way of accomplishing duplexing is to use the cross-coil scheme (Fuk81). This method uses two separate coils for the transmitting and receiving functions. Although this scheme provides good H_1 homogeneity and fast recovery, careful alignment of the coils has to be made and the probe construction is more complicated and bulkier.

Crossed diodes (two parallel diodes pointing in opposite directions) are commonly used to accomplish duplexing because they act like switches: they turn on (low impedance, a few ohms) for large signals and turn off (high impedance, essentially just their capacitance) for small signals. Therefore, by connecting a set of crossed diodes in series

with the transmitter and by putting another set in shunt before the receiver preamplifier one can decouple the transmitter and the receiver.

The tank circuit used in the probe is a parallel resonance LC circuit. A parallel resonance circuit is a high impedance tank circuit with the resonance condition of $\omega^2LC = 1$ (Rah75), where ω is 2π times the resonance frequency (f_0). L is the inductance of the NMR coil, and C is the value of the capacitor in parallel with the coil. The quality factor Q of the tank circuit is defined as $Q = \omega L/R$, where R is the resistance of the coil. A typical NMR coil has a Q of 100 or more.

For the experiments reported here different coils were wound for experiments at different frequencies. For given f_0 and C (typically ~ 150 pf), one can calculate the inductance needed to satisfy the resonance condition $\omega^2LC=1$. The NMR coils of desired value of inductance (in micro-henry) can be wound using the formula (Rah75): $L = n^2r^2/(9r + 10d)$, where n is the number of turns of the coil and r,d are the radius and the length of the coil (both in inches), respectively. The coil inductance and/or the impedance of the tank circuit is measured using an impedance meter. Typically, the parallel resonance tank circuit has an impedance value of $Z = Q\omega L \sim 5000\ \Omega$.

Since the output of the transmitter and the input of the receiver both have impedances of 50 Ω, an impedance matching network is necessary to couple the high impedance tank circuit to the transmitter and the receiver. Two kinds of impedance matching schemes are frequently used. One of the impedance matching schemes is to use capacitive coupling (Cro76, Kan80); this requires two capacitors: one in parallel,

the other in series to the tank circuit. The other impedance matching scheme is to use transformer coupling of the transmitter and the tank circuit; we have a high input impedance preamp so no matching on the preamp is used. A field-effect transistor (FET) Q switch (Con77) is used to reduce the blocking/recovery time of the receiving apparatus in the low frequency experiments.

Several other considerations have to be made when constructing an NMR probe. A good NMR probe should not give rise to spurious signals, such as acoustic coil noise (or " coil disease"), stray spin signals, piezoelectric signals and pick-up of rf interference emitted by the digital equipment in the lab. Usually, proper selection and installation of parts used in contructing the probe prevents such spurious signals. For example, ceramic capacitors which give rise to piezoelectric signals should not be used. Others like the acoustic coil noise can be minimized by winding the rf coil to fit snugly to the sample cell.

Before each experiment, proper procedures were taken to check for spurious signals. Sometimes, improvements in grounding and filtering were made to remove non-coherent noise and/or spurious signals.

2.1.3 Transmitter and RF Field

The transmitter is composed of an rf frequency source, a pulse generator and an rf amplifier to amplify the rf transmitter signal to the desired level (typically several hundred watts peak power).

A General Radio type 1164A coherent frequency synthesizer is the rf source of our super-heterodyned pulse spectrometer. The synthes-

izer has a stable " clock " and an operating range of 0.01 MHz to 70 MHz. The rf phasing and gating are all done at the 30 MHz IF (intermediate frequency) using the fixed 30 MHz output of the synthesizer. This signal is then heterodyned to the operating frequency by mixing against the synthesizer output (at f_0 + 30 MHz). The resulting phased and gated rf is at the desired frequency f_0 (see Fig.2).

A ENI model A300 rf amplifier (class A; i.e. output power is directly proportional to the input power) is used to boost the rf signal. The final transmitter output power is 300 watts (~ 55 dBm). The number of dBm (Rah75) is 10 X $\log(P_f/P_i)$ where P_f is the output power and P_i is 1 mW (a fixed reference value).

An assembly of home-built pulse generators was used in the experiments. Pulse lengths and/or pulse timings may be controlled manually or by a microcomputer. A 90° pulse length $t_{p,o}$ is related to the rf field H_1 by $\gamma H_1 t_{p,o} = \pi/2$. For a given resonance frequency f_0 and power P, the rf field H_1 depends on the Q and the volume V of the transmitter transmitter coil by the relation (Fuk81): $H_1 \simeq 3(PQ/Vf_0)^{1/2}$. A tank circuit with large Q has better H_1 (and hence more stored field energy) for a fixed transmitter power and more received power to the preamplifier for a given precessing magnetization. Usually, the 90° and the 180° pulse lengths were tuned using a liquid sample before each experiment and are held constant throughout the given experiment. Typical H_1 values in this work are in the order of 50 gauss.

As shown in Fig.2, a low-pass filter is placed before the power amplifier to remove spurious high frequency signals generated during

frequency mixing. Furthermore, a high-pass filter was used after the power amplifier to get rid of the low frequency noise from the power amplifier (we drive our ENI power amplifier into non-linearity during rf pulses; the resulting power supply transients appear weakly in its output). Several sets of crossed diodes in the " noise reduction box" after the ENI output serve to improve the isolation of the transmitter from the receiver: this is important since the ENI power amplifier produces lots of wideband noise, even when the rf pulse is absent.

2.1.4 Receiver and Receiver Blocking

The receiver contains four major components: a pre-amplifier, a frequency mixer, an IF amplifier, and a phase-sensitive detector (PSD). The IF amplifier used in our super-heterodyned pulse spectrometer has variable gain; the phase sensitive detection is done in two orthogonal phases.

After the signal has been amplified by the preamp (at f_0 + Δf, where Δf is the bandwidth away from the center carrier frequency), it is sent to the frequency mixer for heterodyning. A heterodyne system has the advantage of performing most of the amplification at a constant intermediate frequency; variable frequency operation is thus easily obtained (Fuk81). The heterodyned signal (at 30 - Δf) is then amplified by the IF amplifier and sent to the PSD (see Fig.2). The output signal after the detector is the desired NMR signal (at - Δf), which is usually called the audio signal. The in phase and quadrature audio signals then go through a dual RC filter to remove high frequency noise and are then sent to the transient digitizer.

In pulsed NMR experiments, one of the common problems is the receiver blocking (also called the deadtime) during which the early part of the NMR signal is obscured. The cause of the deadtime is the combination of the transmitter pulse, the ringing of the LC circuits, and the recovery (from such severe overload) of the receiver. The deadtime causes a fundamental problem in fourier transforming the NMR signal and hence affects the measurement of moments, especially when the line is broad. Though there are pulse sequences (e.g. magic echo pulse sequence) (Rhi70, How82) to get away from the deadtime, the signature of the deadtime can not be eliminated. However, it can be minimized by Q-switching, by crossed diode protection and by minimizing the receiver recovery time (Fuk81). Typical deadtimes in this report are ~ 30 μs when running high field (14.7 MHz) experiments, becoming ~ 80 μs at very low frequency (1.256 MHz).

2.1.5 Data Acquisition and Manipulation

A transient digitizer, Biomation 2805M, was used to digitize the dual audio frequency signals. The maximum conversion rate of the biomation is 5 MHz with memory size of 2 K (2048) 8-bit words per channel. One half of the digitized signal (i.e. 1024 × 8 bits per channel) is transfered to the Apple II microcomputer for data acquisition, signal averaging, and data storage. The Apple II computer is also connected to the pulse generator for pulse sequence timing. Experimental data were stored on diskettes for permanent record. The Apple II computer is also used for data analysis and fourier transforming the transient signal.

2.2 CRYOGENIC SYSTEM AND TEMPERATURE MEASUREMENT

The cryogenic system, namely the low temperature dewar and the low temperature probe served to regulate the temperature of the sample under study from 4 K up to room temperature. The temperature range of the studies reported were determined by the phase transition temperature of the sample under investigation.

For the α-CO experiments, data below the α-β transition temperature ($T_{\alpha\beta}$ = 61.55 K) were examined. In the CO_2 experiments, data were taken from about 150 K up to the melt (T_m = 216.56 K). Different thermometers were used for the two experiments; details will be given later.

2.2.1 Low Temperature Dewar

The low temperature dewar (Fig.4) used is a liquid helium, gas flow, variable temperature dewar. The dewar has inner and outer wells; each is vacuum insulated. During the α-CO experiments, the inner well was filled with liquid helium (4.2 K) and the outer well was filled with liquid nitrogen (77.3 K) for double shielding. In the CO_2 experiments, the inner well was filled with liquid N_2 and the outer well was left empty.

A vacuum pump and/or a U-shaped liquid N_2 cryo-pump (Fig.4) were used to maintain the vacuum of the dewar. The liquid N_2 cryo-pump contained grained charcoal of high surface area to adsorb out-gas in the system. It can hold vacuum without the vacuum pump on the order of 6 to 8 hours, and was only used during the CO_2 experiments. For α-CO experiments, the vacuum valve on the dewar is shut once vacuum in

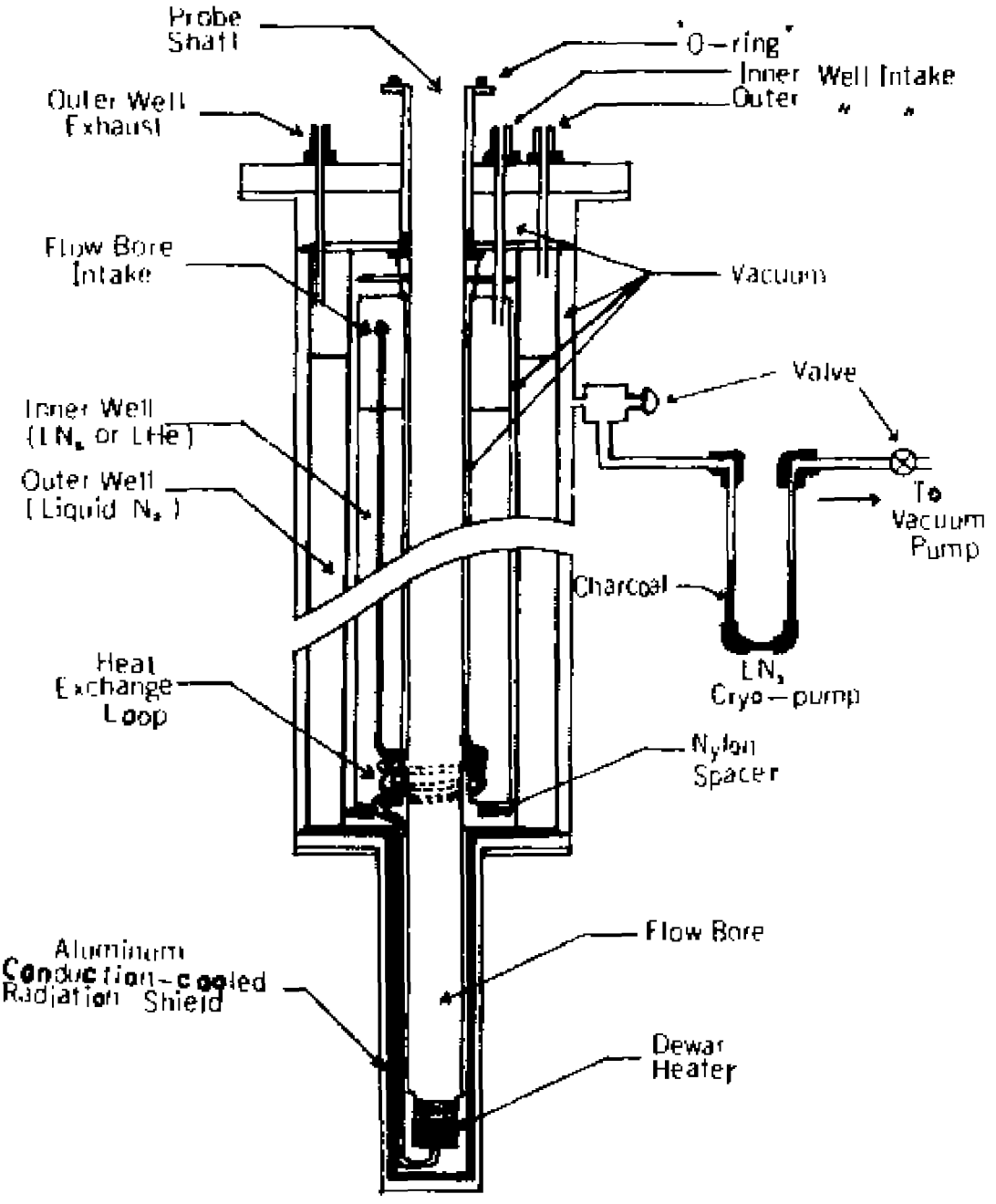

Figure 4: Schematic drawing of the low temperature (LN_2, LHe) dewar.

the dewar is established. This is because liquid He itself is an excellent cryo-pumping agent.

The temperature of the sample is that of the flowing gas in the flow bore (see Fig.4). Cold vapor is forced into the flow bore intake by a small positive pressure in the inner well. It is cooled by the liquid in the inner well when it passes through the heat exchange loop at the bottom of the inner well. The cold vapor is then passed through the dewar heater which is powered by a Cryodial proportional temperature controller (Cryotronic, Inc.) set to the desired temperature. The heated vapor finally passes up the flow bore and around the the sample chamber and exits at the top of the dewar via the exhaust line of the probe.

The vapor flow rate is measured and controlled by several commercial flow meters and a fine flow valve, respectively. The flow meters and flow valve were installed in series with the exhaust line on the probe connected by rubber hoses. A 30 psig pressure gauge indicates the pressure of the inner well. Several pop-off valves are also installed to prevent the inner well from becoming over-pressurized. Furthermore, an adjustable flow-sensing switch is also installed in series with the flow meters to turn off the power to the dewar heater when the exhaust vapor flow is too low due to a flow bore block or an empty inner well. This safety feature prevents burning out the heater or melting its solder joints.

During the CO_2 experiments, the inner well was pressurized by external N_2 gas. We installed a gas line from the liquid N_2 storage tank outside the building in series with a control valve to our lab. We also put a container of Drierite in series with the external N_2 gas

line to absorb water (which had produced annoying blocks in the gas flow circuit of the dewar). Typically, the external flow rate is adjusted to give an inner well pressure of 2 psig; the flow meter on the flow bore read 4 standard cubic feet per hour (SCFH). The liquid N_2 in the inner well usually lasted 12 ~ 15 hours per transfer (approximately 3 liters).

No external pressure was needed in the α-CO (low temperature) experiments. Typically, the inner well pressure was determined by a low pressure relief valve, the pressure ran at about 0.5 psig. The flow in the flow bore was ~ 1.0 SCFH and the inner well exhaust flow was ~ 1.5 SCFH. Normally, the liquid He in the inner well needed to be refilled every 24 hours or so, and the shielding liquid N_2 in the outer well was refilled every 6 ~ 8 hours.

Typical heat controller and flow settings for various temperatures in the two experiments are listed in Appendices A and B.

2.2.2 Low Temperature Probe

The home-built low temperature NMR probe is shown in Fig.5. A 1/16 inch I.D. thin-wall stainless steel tubing served as the gaseous sample fill line and was connected to the gas supply rig (Fig.6) with a Cajon O-ring fitting.

Samples were held in a 1.5 cc nylon sample chamber which was sealed to a copper nipple by differential contraction. The NMR coil fit snugly on the sample chamber and was held by a teflon coil holder.

Another thin-wall stainless steel tubing (5/16 inch I.D.) served as the rf transmission line. The rf wire inside this tube is

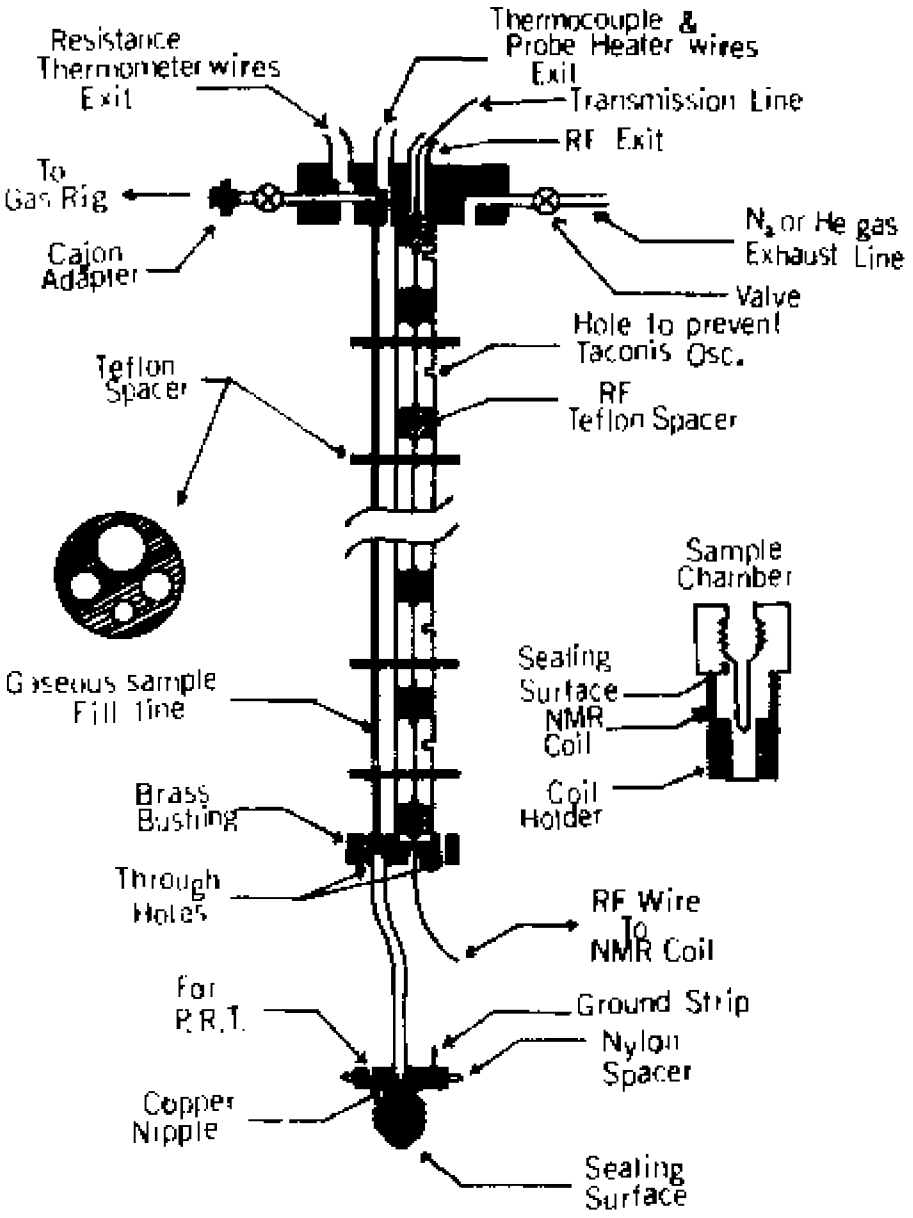

Figure 5: Schematic drawing of the low temperature probe and NMR sample chamber.

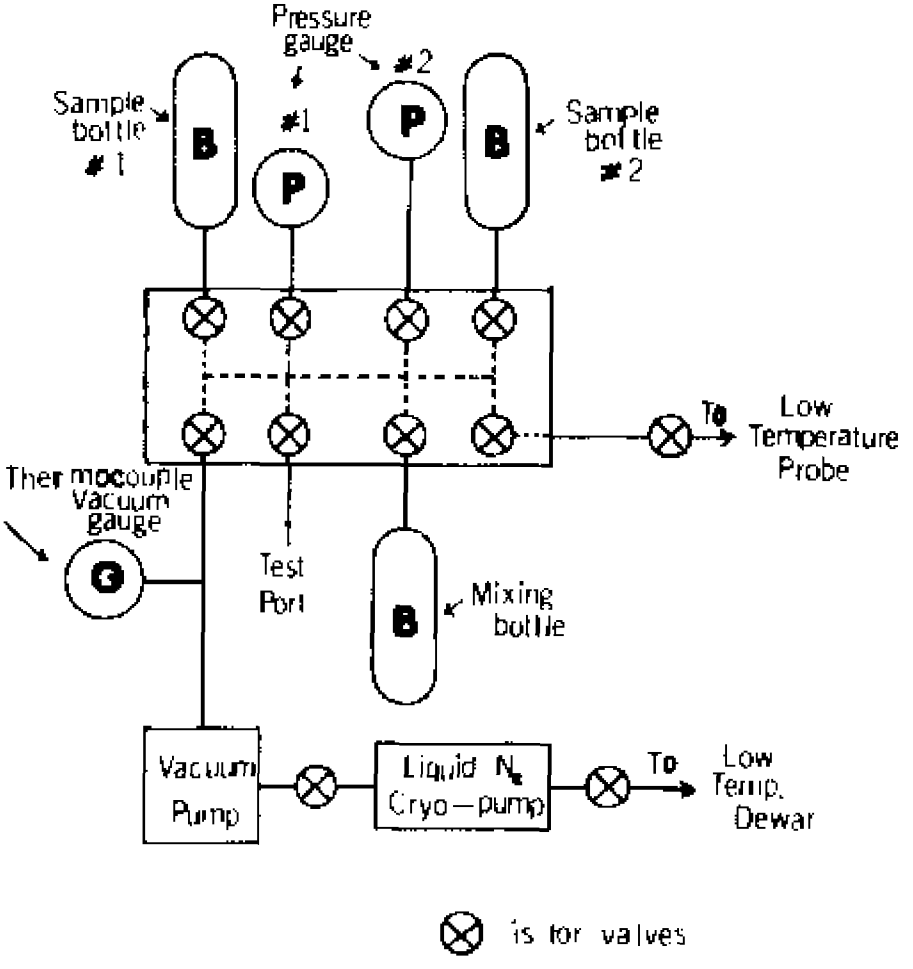

Figure 6: Schematic of the gas supply rig and the vacuum system. The connections to the cryogenic system are also shown.

insulated with teflon tubing and is held rigidly by a string of teflon spacers. The rf wire is connected to a sealed BNC connector on top of the probe. Several slots were cut into the side of the 5/16 inch stainless steel tubing to prevent Taconis oscillations (Sco59).

As shown in Fig.5, there are two outlets at the top of the probe for thermocouple wires, probe heater wires and resistance thermometer wires (wires not shown in the figure). They are sealed with 5-minute Epoxy at the top of the probe; these seals are leak-tight.

The resistance thermometer is a four-wire potentiometric scheme; four separate wires extend to a position right above the brass bushing (Fig.5) and are connected to the resistance thermometer by pin connectors. The thermometer is placed in a hole on the copper nipple so that the temperature of the sample can be determined accurately.

A copper-constantan thermocouple wire was also used for temperature measurement and extended to the copper nipple where it was soldered for good thermal anchoring. Another copper-constantan thermocouple wire, which wound around the sample fill line down 2/3 of the total length of the probe, is used as a probe heater. Running this heater established an upwards temperature gradient in the dewar's flow bore; for the volatile samples used here this was an easy way of keeping the sample from moving around in the probe due to vapor phase transport.

Several evenly spaced teflon spacers are designed to separate the two stainless steel tubes; there are additional holes (see Fig.5) for the thermometry wires. The spacers also served to prevent direct contact of the tubes with the dewar.

The overall length of the probe is about 43 and 7/8 inches long from the bottom of the top hat to the center of the sample chamber. This length has been carefully measured so that the sample chamber is at the center of the magnet when the probe sits in the dewar.

2.2.3 Temperature Measurement

As mentioned earlier, the thermometry consists of a copper-constantan thermocouple and a platinum resistance thermometer (PRT) or a calibrated Lake Shore carbon-in-glass resistor. A variable current power supply provided the resistors with low currents (1.4, 4, 16, 35 or 104 micro-amps). The voltages from the four-wire potentiometric resistance determination and from the thermocouples were read by a digital voltmeter capable of resolving microvolts.

The PRT was most useful above 50 K and was used in the CO_2 experiments; the temperature reading was taken directly from a calibrated resistance vs. temperature table. In the α-CO experiments (30 to 60 K), the carbon-in-glass resistor was used. In both experiments, temperature readings from the resistance thermometer were always confirmed by the copper-constantan thermocouple readings.

The temperatures determined from the above set-up are believed accurate to $\pm$ 0.2 K. Since typical laboratory time per data point was 2 ~ 12 hours, all data present in this report are believed accurate to $\pm$ 0.5 K due to small temperature drifts in the course of the experiment.

2.3 SAMPLE PREPARATION

All the sample gases used in this report are listed in Table II. Some of the experiments required high concentrations of C^{13} spins; such samples were directly taken either from the 90% C^{13} enriched CO gas bottle or from the 99% C^{13} enriched CO_2 bottle. For experiments of low C^{13} concentration, samples were prepared by mixing the high C^{13} concentration gas with the natural C^{13} abundance gas at room temperature. Details will be given in this section.

2.3.1 Gas Rig

The gas rig is shown schematically in Fig.6 and is self-explanatory. The gas rig manifold (dotted line in Fig.6) consists of several " T" and " CROSS" swage connectors joined to 1/4 inch copper tubings. There are eight outlet ports on the gas manifold, each controlled by a valve. A pair of Cajon O-ring fittings is used in front of each outlet port for easy connection and/or replacement of gas bottles. The gas rig has three bottle mounts and several ports that are interchangable.

A vacuum pump equipped with a thermocouple vacuum gauge served to pump the experimental set-up (the gas rig, the probe and the low temperature dewar). The entire vacuum system was checked before every run by a Veeco mass spectrometer leak detector (model MS-9). The leak detector operates under high vacuum and can detect very small leaks; it has apprehended several leaks. The leak detector is explained in its instruction manual.

TABLE II

List of Gas Bottles Used in the Experiments

SAMPLE BOTTLE	C^{13} SPIN ENRICHMENT	PRODUCT DESCRIPTIONS
$C^{13}O$	90%	Merck
CO*	1.108%	Matheson[J]
$C^{13}O_2$	99%	Prochem
CO_2*	1.108%	Matheson**
O_2	-----	Matheson[J]

*Natural abundance.

[J]Research purity 99.99%.

**Research purity 99.995%.

2.3.2 Sample Mixing and Sample Transfer

Two C^{13}-NMR experiments are presented here, namely the n-CO and CO_2 experiments. In each experiment, samples of both high C^{13} abundance and low C^{13} concentration were needed. All samples were prepared (or mixed) in a 150 cc stainless steel mixing bottle before transfering into the NMR sample chamber.

For the low C^{13} concentration experiments, samples were obtained by mixing C^{13} enriched gas with gas of natural C^{13} abundance at room temperature. The additivity of partial pressures and ideal gas behavior were assumed in computing the concentrations. The pressure readings were taken directly from the pressure gauges mounted on the gas rig.

During the CO_2 experiments, samples were first transferred from the stainless steel mixing bottle into the 1.5 cc nylon sample chamber in the liquid phase. In the first experiments, we found that the spin-lattice relaxation time (T_1) of solid CO_2 was too long (on the order of several hours) for signal averaging. We therefore added a small amount of O_2 to the sample to reduce T_1 to ~ 100 s at 150 K. In order to accomplish this, the liquid CO_2 sample was first cooled to the solid phase at ~ 120 K (where the vapor pressure is essentially zero), then approximately two atmospheres of O_2 were addded on top of the solid CO_2. The sample was warmed up into the liquid phase and allowed to stand for typically two hours for the O_2 gas to dissolve into the liquid CO_2. By checking with the NMR signal of the liquid CO_2 sample, we concluded that the O_2 added to the sample reduced the

C^{13} T_1 in the liquid from ~ 50 s (O_2-free samples) to ~ 2 s. In order to form a good poly-crystalline powder sample, the O_2-doped sample was frozen by pulling the probe out of the research dewar and immersing the sample chamber into a liquid N_2 vessel. This was done practically within seconds. Finally, the probe was returned back to the dewar at ~ 130 K and the residual O_2 gas was pumped out. Our experimental data indicate that the O_2 gas dissolved in the solid CO_2 sample stayed in solution, except at temperatures near the melt where T_1 was observed to lengthen over a period of many hours (presumeably the O_2 was leaving the solid).

During the CO experiments, no O_2 was added to the sample intentionally since earlier NMR measurements indicated that the sample already contained a small amount of O_2: at 50 K, T_1 ~ 50 s vs. T_1 ~ 150 s (O_2-free samples). The sample was first condensed from the stainless steel mixing bottle into the sample chamber in the liquid phase. Then, it was cooled into the β-phase solid and then further cooled to the α-phase, generally within 15 minutes. The CO samples prepared in this manner appeared not to form perfect poly-crystalline powder samples; details will be seen in Chapter V.

Chapter III

SPIN INTERACTIONS

3.1 BACKGROUND

Solids α-CO and CO_2, the subjects of this report, share the same Pa3 crystal structure. The molecular properties and phase diagrams of the solids are described in Chapter I.

In the orientationally ordered Pa3 structure solids, a molecule that jumps to a previously vacant neighboring site reorients through a tetrahedral angle. The C^{13} NMR experiments reported here detect these combined translational-rotational jumps in α-CO and CO_2. This chapter is a discusion of the spin interaction mechanisms that dominate the spin relaxation in these molecular solids. The experiments and the related pulse techniques will be presented in Chapter IV.

3.2 SPIN RELAXATION MECHANISMS

There are two principal line broadening mechanisms that are effective in both $C^{13}O$ and $C^{13}O_2$ solids: the chemical shift anisotropy (CSA) and the intermolecular dipole-dipole interaction between the C^{13} spins.

Both $C^{13}O$ and $C^{13}O_2$ solids have only one spin species per molecule; the C^{13} like-spin intramolecular dipole interactions are absent. Although O^{17} spins (I = 5/2, natural abundance 0.037%) are likely to be present in both materials under study, their abundance

is much smaller than the C^{13} concentration and thus the effect of the unlike-spin dipolar interaction can be neglected. Because the C^{13} nucleus has spin 1/2, the electrical charge distribution in the nucleus has no electrical quadrupole moment to contribute to the relaxation.

We shall briefly describe the two interactions (CSA and dipolar interaction) in this section.

3.2.1 Chemical Shift Anisotropy Interaction

The chemical shift arises from the orbital motion of the electrons in a molecule (or atom) under the influence of the applied static field H_0. The field H_0 produces an electronic current in the molecule (or atom), and the induced current then creates a small magnetic field ΔH at the nucleus. The general theory of the chemical shift was given by Ramsey (Ram50) and formal treatment of the theory has been given by standard texts (Sli80, Abr83).

The direction and the magnitude of this field ΔH felt by the nucleus depend on the electronic structure of the molecule, hence the name " chemical shift ". The field ΔH is different for different molecular orientations relative to the external field H_0. The nuclei see a magnetic field ΔH in addition to the field H_0; the spin frequency ω is given by

$$\omega = \gamma |\vec{H}_0 + \Delta\vec{H}| \qquad (1)$$

where $\Delta\vec{H} = \bar{\bar{\sigma}}\vec{H}_0$ and $\bar{\bar{\sigma}}$ is a second rank tensor. We note that the chemical shift is linearly proportional to H_0 and should

in general depend upon the orientation of the molecule with respect to H_0. The x, y, and z co-ordinate frame may be chosen to coincide with the principal axes of the shift tensor; in this case the σ-tensor becomes diagonal with principal components σ_{xx}, σ_{yy}, and σ_{zz}. Then ΔH can be written as

$$\Delta H = \begin{pmatrix} \sigma_{xx} & 0 & 0 \\ 0 & \sigma_{yy} & 0 \\ 0 & 0 & \sigma_{zz} \end{pmatrix} \begin{pmatrix} H_{x0} \\ H_{y0} \\ H_{z0} \end{pmatrix} = \begin{pmatrix} \sigma_{xx}H_{x0} \\ \sigma_{yy}H_{y0} \\ \sigma_{zz}H_{z0} \end{pmatrix} \qquad (2)$$

and by applying Eq.(1), we find

$$\begin{aligned} \omega^2 &= \gamma^2(\vec{H}_0+\Delta\vec{H})\cdot(\vec{H}_0+\Delta\vec{H}) \\ &= \gamma^2\left[H_0^2+2(\Delta\vec{H}\cdot\vec{H}_0)+\Delta H^2 \right] . \end{aligned} \qquad (3)$$

The ΔH^2 term is a second order term and hence can be neglected because chemical shift are small (~ 100 ppm). Now carrying out the dot product using Eq.(2), the above Eq.(3) becomes

$$\begin{aligned} \omega^2 &= \gamma^2 H_0^2\left[1 + 2\sum_j \sigma_{jj}(H_{j0}/H_0)^2 \right] \\ &= \gamma^2 H_0^2\left[1 + 2\sum_j \sigma_{jj}\cos^2\gamma_j \right] \\ &\approx \gamma^2 H_0^2\left[1 + \sum_j \sigma_{jj}\cos^2\gamma_j \right]^2 . \end{aligned} \qquad (4)$$

where $H_{j0}^2 = (\hat{j}\cdot\vec{H}_0)^2 = H_0^2\cdot\cos^2\gamma_j$, j = x, y, and z; the $\cos\gamma_j$ are the direction cosines expressing the orientation of the three principal axes with respect to H_0. It may be useful to define $\sigma_0 = (1/3)\sum_j \sigma_{jj}$ (i.e. isotropic shift), j = x, y, and z. Together with the condition $\sum_j \cos^2\gamma_j = 1$, Eq.(4) then gives (Blo55)

$$\omega = \omega_0\left[1+ \sigma_0 + \sum_j \sigma_{jj}\{\cos^2\gamma_j-(1/3)\}\right] .$$

Specifically, for molecules that have an uniaxial symmetry (such as CO and CO_2 studied here), so that $\sigma_{xx} = \sigma_{yy} = \sigma_\perp$ and $\sigma_{zz} = \sigma_{/\!/}$, the precession frequency is then given by

$$\begin{aligned}\omega &= \gamma H_0 \left[1 + \sigma_{/\!/}\cos^2 \theta + \sigma_\perp(1 - \cos^2 \theta)\right] \\ &= \gamma H_0 \left[1 + \sigma_0 + \Delta\sigma \ (\cos^2 \theta - \{1/3\})\right]\end{aligned} \qquad (5)$$

where $\theta=\gamma_z$ and $\sigma_0 = (\sigma_{/\!/} + 2\sigma_\perp)/3$ represents the isotropic shift (such as in a liquid). In liquid, rapid molecular tumbling causes the averaging of $\langle\cos^2\theta\rangle$ to 1/3; hence there is no anisotropic shift. $\sigma_{/\!/}$ and $\sigma_\perp$ are the shift values parallel and perpendicular to H_0, respectively; $\Delta\sigma = \sigma_{/\!/} - \sigma_\perp$ is the shift anisotropy. In this case, the resonance frequency depends on only one angle, θ.

The powder pattern lineshapes which appear in C^{13} spectra of CO and CO_2 solids have been calculated by Bloembergen and Rowland (Blo55), Spiess and Haeberlen (Spi74, Hae76) and Mehring et al. (Meh71, Meh76). Assuming that the resonant absorption at a given frequency ω is given by $G(\omega)$, $G(\omega)d\omega$ is proportional to the number of spins in the absorption spectrum whose frequency lie between ω and $\omega + d\omega$. Correspondingly, assume that $N(\theta)d\theta$ is the number of spins whose angle is between θ and $\theta + d\theta$, where ω corresponds to θ and vice versa. Then

$$G(\omega)d\omega = N(\theta)d\theta$$

$$\text{or} \quad G(\omega) = N(\theta) \ |d\omega/d\theta|^{-1}. \qquad (6)$$

Assuming a random distribution on the unit sphere, then

$$N(\theta) = (1/4\pi)\, 2\pi \sin\theta\, d\theta$$
$$= (1/2)\sin\theta\, d\theta \ ;$$

the constant 4π in the denominator is the normalization factor. By applying Eq.(5), taking $\omega_0 = \gamma H_0$, we get

$$\left|d\omega/d\theta\right|^{-1} = 2\Delta\sigma\, \omega_0\, \cos\theta\sin\theta d\theta \ .$$

Then Eq.(6) becomes

$$G(\omega) = \left\{ 4\Delta\sigma \cdot \omega_0 \cdot \cos\theta \right\}^{-1} \ . \qquad (7)$$

Furthermore, from the upper equation of Eq.(5), one finds

$$\cos\theta = \left[(\omega - \omega_\perp)/\omega_0\, \Delta\sigma\right]^{1/2} \ ,$$

where $\omega_\perp = \omega_0(1 + \sigma_\perp)$, which we plug into Eq.(7) to get

$$G(\omega) = (1/4)\left[\omega_0\Delta\sigma(\omega - \omega_\perp)\right]^{-1/2} \ . \qquad (8)$$

We see that $G(\omega)$ diverges when $\omega = \omega_\perp$. The uniaxial powder pattern of α-CO and CO_2 solids will be shown in Chapter V.

3.2.2 Dipolar Interaction

The dipolar interaction considered here is a like-spin term. The Hamiltonian can be written as (Sli80, Abr83):

$$\mathcal{H}_D = \frac{1}{4}\gamma^2\hbar^2 \sum_{\substack{j,k \\ j\neq k}} \frac{(1 - 3\cos^2\theta_{jk})}{r_{jk}^3}\left[3I_{zj}I_{zk} - \vec{I}_j \cdot \vec{I}_k\right] \qquad (9)$$

where θ_{jk} is the orientation of the vector $\vec{r}_{jk}$ from spin j to spin k with respect to the direction of H_0, and the z-axis is parallel to the applied field.

In the rigid lattice limit, the Van Vleck calculation of the like-spin dipolar part of the second moment (Van48, Abr83) is

$$M_2 = \frac{3}{4}\gamma^4\hbar^2 I(I+1) f \sum_k \frac{(1 - 3\cos^2\theta_{jk})^2}{r_{jk}^6}, \qquad (10)$$

where f is the fractional concentration of the magnetic nuclei. For a powder made of crystallites of random orientations, one averages the $(1 - 3\cos^2\theta_{jk})^2$ over all orientations , yielding a factor of 4/5 and leading to

$$M_2 = \frac{3}{5}\gamma^4\hbar^2 I(I+1) f \sum_k \frac{1}{r_k^6}. \qquad (11)$$

3.3 MOLECULAR MOTIONS AND SPIN INTERACTIONS

The two principal line broadening mechanisms described above can be summarized as follow: The shift anisotropy is proportional to the applied field H_0 and depends on the orientation of the molecular axis with respect to H_0 but is independent of the C^{13} concentration. On the other hand, the dipolar interaction is independent of H_0 but increases with increasing C^{13} concentrations. Consequently, at high field and low C^{13} enrichment the shift anisotropy is the larger interaction, while at low field and high C^{13} enrichment the dipolar interaction dominates.

Experimentally, the rigid (cold) powder pattern linewidths at high field (14.7 MHz) are found to be 5200 Hz and 4780 Hz for α-CO (10% C^{13}) and CO_2 (15% C^{13}) solids, respectively. By comparison, the high field spectra of high C^{13} concentration samples show that the dipolar interaction only served to broaden the powder lineshape but did not change the overall linewidth in the rigid lattice limit. This indicates that at high field the shift anisotropy is indeed dominating the spectra. At low field (1.256 MHz), the rigid lattice linewidths ($\Delta\omega_{RL}$) at full width and half maximum intensity (FWHM) are 960 Hz and 1120 Hz for α-CO (90% C^{13}) and CO_2 (99% C^{13}), respectively. The shift anisotropies scale to 444 Hz for α-CO and 410 Hz for CO_2 at low field (1.256 MHz) regardless of the C^{13} concentration. Since linewidths from different sources typically add as squares ($\Delta\omega^2 = \Delta\omega^2_{dipole} + \Delta\omega^2_{CSA} + \ldots$), the dipolar interaction is seen to be dominant, as expected. For both high and low field experiments, line narrowing was observed at high temperature (except α-CO at

high field); detailed discussion and analysis will be presented in Chapter V.

It will be shown later that the rate of the translational jumps and the rotational jumps can be separately determined due to the above described fundamental differences in the two interactions.

3.3.1 Molecular Rotation

In the Pa3 solids, the rotational jumps (considerd apart from the translational part of the motion) between the body diagonals of the cube will modulate the chemical shift anisotropy. Rapid reorientations between the body diagonals will average the chemical shift anisotropy to zero. To show this, we define the normalized unit vectors

$$\hat{n}_1 = (1, 1, 1)/\sqrt{3}$$

$$\hat{n}_2 = (1,-1, 1)/\sqrt{3}$$

$$\hat{n}_3 = (1, 1,-1)/\sqrt{3}$$

$$\hat{n}_4 = (1,-1,-1)/\sqrt{3} \quad ,$$

$$\hat{H}_0 = (x, y, z), \quad \text{where } x^2+y^2+z^2 = 1 \ ,$$

corresponding to the four body diagonal axes and external field axis, respectively. The average of $\cos^2\theta$ is:

$$\begin{aligned} \langle \cos^2\theta \rangle &= (1/4)\sum_j (\hat{H}_0 \cdot \hat{n}_j)^2 \\ &= (1/4)\sum_j \cos^2\theta_j \qquad (j = 1, 2, 3, 4) \\ &= (1/4)(1/3)\left[(x+y+z)^2 + (x+y-z)^2 \right. \\ &\qquad \left. + (x-y+z)^2 + (x-y-z)^2 \right] \\ &= (1/4)(1/3)\left[4(x^2+y^2+z^2) \right] \\ &= 1/3 \ , \end{aligned} \tag{12}$$

thus $\langle \cos^2\theta - (1/3) \rangle_{avg} = 0$.

and hence the anisotropic chemical shift appearing in Eq.(5) is averaged to zero.

In α-CO , the distance between molecular centers is 0.398 nm (nearest-neighbor distance) (Koh60), much larger than the distance from the C^{13} to the molecular center (~ 0.057 nm, roughly 1/2 of the C-O bond length) (Koh60). Hence, rotational jumps between the body diagonals will slightly reduce the intermolecular dipole-dipole interactions. The rotations will not modulate the dipolar interaction in CO_2 solid because the C^{13} spin is always at the molecular center and is not displaced by pure rotations.

Thus, the rotational jumps can be observed at high field with low C^{13}-enriched samples through the modulation of chemical shift anisotropy.

3.3.2 Molecular Translational Diffusion

Molecular translational jumps, if considered separate from the rotations, will modulate the dipolar interaction to zero if sufficiently rapid. On the other hand, translational motion alone, will not modulate the chemical shift anisotropy interactions, which depends only on molecular orientation. Hence, the translational jumps can be detected at low field and high C^{13} enrichment through the modulation of dipole-dipole interactions.

Bloembergen, Purcell, and Pound (BPP) showed (Blo48) that a fluctuating dipolar field (i.e. a change in the local field H_L) caused by atomic diffusion or molecular rotation can induce transitions among

Zeeman levels and thus relax the spins. They treat the fluctuating dipolar Hamiltonian (Eq.9) as a perturbation on the Zeeman levels, assuming an exponential correlation function. They showed (Blo48) that the diffusion contribution to the relaxation rate $(T_1)_d^{-1}$ is related to the dipolar linewidth ω_d and the Larmor frequency ω_0 by (Ail71)

$$(T_1)_d^{-1} \approx (\omega_d)^2\tau_c/(1 + \omega_0{}^2\tau_c{}^2) \ . \qquad (13)$$

where τ_c is the correlation time for the motion (i.e. the mean time between atomic jumps). Eq.(13) was derived based on the assumption that τ_c is much smaller than the relaxation time; that is, it requires many atomic jumps to relax a spin (weak collision). From Eq.(13), we note that a $(T_1)_d$ minimum occurs when $\omega_0\tau_c \approx 1$; the local dipolar enviroment appears nearly static to the precessing nuclear spins and hence produce the most rapid spin-lattice relaxation. Furthermore, on the high temperature side of the $(T_1)_d$ minimum ($\omega_0\tau_c << 1$), $(T_1)_d$ is independent of the frequency ω_0 whereas on the low temperature side of the minimum ($\omega_0\tau_c >> 1$), $(T_1)_d$ is propotional to $\omega_0{}^2$. The BPP (weak collision) theory is valid in the motionally narrowed state ($\tau_c << T_2 = 1/\Delta\omega_{RL}$; $\Delta\omega_{RL}$ is the rigid lattice linewidth HWHM expressed in angular frequency units), even in a weak applied field (Ail71).

In the rigid lattice limit ($\tau_c >> T_2$) and when the fluctuating dipolar field is comparable to or greater than the applied field, then the dipolar Hamiltonian can no longer be treated as a perturbation of Zeeman levels, and hence the weak collision theory is no longer valid (Sli64, Ail71). In this case, the correlation time τ_c is comparable

to the relaxation time, therefore only one atomic jump is needed to relax a spin (strong collision). The strong collision theory of low field relaxation and ultraslow motions is derived by Slichter and Ailion (SA) (Sli64, Ai171), and has been widely used. The SA (strong collision) theory was developed based on two assumptions. The first assumption is that the applied field is small enough so that the Zeeman and dipolar system can couple strongly, therefore a common spin temperature (Red55, Sli80, Abr83) is established between each jump (that is, assuming $\tau_c >> T_2$). The second assumption is the so called sudden approximation; that is, the time a nucleus spends in the actual process of jumping is assumed to be short compared to its precession period so that the spin orientation is the same immediately before and after the jump. Since the actual time a nucleus spends in jumping is approximately a lattice vibration period ($\sim 10^{-12}$ s) and the Larmor period is typically four or five order of magnitude longer; we see that the sudden approximation is quite good.

For the like-spin dipolar interaction in the field H_1 (the rotating field), SA theory predicts (Ai171)

$$\frac{1}{T_1\rho} = \frac{2(1-p)}{\tau_c} \frac{H_D^2}{(H_1^2 + H_D^2)} , \qquad (14)$$

where $T_1\rho$ is the spin-lattice relaxation time in the rotating frame, H_D is the dipolar local field, and (1-p) is a geometric factor of order unity which characterizes the fractional change in spin energy resulting from a diffusion jump.

Experimentally, the relaxation time in low field ($T_1\rho$) can be determined using various NMR techniques, such as the ADRF method (Sli61), the spin-locking method (Har62), and the phase-shifted pulse technique (Jee67).

In the ADRF (adiabatic demagnetization in the rotating frame) method (Sli80, Sli61), the static field H_0 is displaced from resonance intentionally, then an rf field (H_1) is turned on while H_0 is off resonance, the static field is then allowed to return to resonance adiabatically. Since the magnetization is always parallel to the effective field ($\vec{H}_{eff} = \vec{H}_0 + \vec{H}_1$), in the ADRF method the magnetization ends up parallel to H_1 so that relaxation in very low fields (H_1 typically on the order of several gauss) can be obtained. For the spin-locking ($90^\circ_x - \tau_y$ sequence) method (Har62, Sli80), the magnetization is made to lie along H_1 by applying a 90° pulse followed by an H_1 pulse of variable duration which has a 90° phase shift with respect to the 90° pulse. The relaxation time $T_1\rho$ is determined by the dependence of the magnitude of the magnetization on the duration of the rf pulse. The ADRF and spin-locking methods described above have the advantage that the dipolar signal can be detected with great efficiency. However, these two methods both require rf transmitters which can deliver long, high power pulses (say, on the order of many seconds) which is usually not available in most laboratories.

An alternative way of measuring the dipolar relaxation time is by the phase-shifted pulse technique developed by Jeener and Broeksert (Jee67). The Jeener-Broeksert pulse sequence was used in this report to measure T_{1D} (the spin-lattice relaxation time in the dipolar ordered

state) which corresponds to the dipolar relaxation time measurement in zero field ($H_1 = 0$) and will be presented in Chapter IV. The relaxation time T_{1D} is equal to the diffusion contribution to $T_1\rho$ obtained at $H_1 = 0$, therefore Eq.(14) becomes

$$\frac{1}{T_{1D}} = \frac{1}{\tau_c} 2(1 - p) \ . \qquad (15)$$

Hence, the rate of the translational jumps determined by the T_{1D} measurement can be described by Eq.(15) using the strong collision theory of Slichter and Allion.

3.3.3 Head-Tail Flips

Head-tail (180^0) flips which occur in α-CO (Nar82) will not modulate the shift anisotropy, because the anisotropic shift has a cosine square angle dependence (Eq.5). However, the 180^0 flips will slightly reduce the dipolar interaction strength in α-CO because the C^{13} spins are not at the molecular centers. But, in the temperature range of the α-CO experiments ($45 < T < 62$ K), the rate of the head-tail flips (Nar82) is always large ($\omega_{HT} \sim 4 \times 10^7$ s^{-1} at 45 K and $\sim 4 \times 10^9$ s^{-1} at 62 K) compared to the NMR linewidths ($\lesssim 10^4$ s^{-1}). Thus, the head-tail flips are " invisible " in the experiments described here.

The head-tail flips are not as likely to be present in solid CO_2. Because the CO_2 molecule is physically longer than CO and the lattice parameter of CO_2 ($a \sim 5.55$ °A at $T \sim 20$ K)(Kee34) is smaller than that of CO ($a \sim 5.65$ °A at $T \sim 20$ K)(Kru73), CO_2

molecules are not as 'free' to flip as CO molecules are. The 180° flips are found to be absent in N_2O (Nar82); it seems reasonable that the 180° flips are also absent in the isoelectronic CO_2.

It is interesting to note and we show below that the jump rotations between the body diagonals cannot be observed by dielectric studies. To see this, let us compare the dielectric susceptibilities χ of (a) a system of dipoles which are free only to make 180° flips, (b) a system of dipoles which are free to reorient isotropically, and (c) a system of dipoles which are free to lie along the four body diagonals of a cube. These represent (a) α-CO without the translational-rotational jumps, (b) β-CO, and (c) α-CO with translational-rotational jumps [actually, such a model neglects the restriction that the four sub-lattices are exactly equally occupied; with this restriction, α-CO really belongs to case (a)].

The energy of a molecule of permanent dipole moment $\vec{p}$ in an electric field $\vec{E}$ is

$$\varepsilon = - \vec{p} \cdot \vec{E} = - \mu E \quad ,$$

where $\mu = p\cos\theta$ and θ is the angle between $\vec{p}$ and $\vec{E}$. The average polarization $\vec{P}$ is related to E and χ by (in CGS units)

$$\langle P \rangle = N\langle \mu \rangle = \langle \chi \rangle E \quad ,$$

where N is the number of molecules per unit volume.

In case (a), there are two possible orientations (up or down hereby denoted by + and - , respectively) which differ by 180° and each corresponds to $\varepsilon_+ = \mu_+ E = - Ep\cos\theta$ and $\varepsilon_- = \mu_- E = + Ep\cos\theta$, respec-

tively. Let the probabilities of finding a molecule in the 'up' and 'down' state be W_+ and W_-, respectively, and

$$W_+ = \frac{e^{-\beta\varepsilon_+}}{e^{-\beta\varepsilon_+} + e^{-\beta\varepsilon_-}}$$

$$W_- = \frac{e^{-\beta\varepsilon_-}}{e^{-\beta\varepsilon_+} + e^{-\beta\varepsilon_-}} \quad .$$

where $\beta = 1/kT$, k is the Boltzmann constant and T is the absolute temperature. Then a classical calculation of $\langle \chi \rangle$ for a given molecular orientation (i.e. given θ) can be derived as

$$\begin{aligned} \langle \chi \rangle_a &= (N/E)\left[\mu_+ W_+ + \mu_- W_-\right] \\ &= (Np\cos\theta/E)(W_- - W_+) \\ &= (Np\cos\theta/E)\tanh(\beta\varepsilon) \quad . \end{aligned}$$

At high temperature ($\beta\varepsilon \ll 1$, as always true in our system), the thermal average of χ in case (a) is then

$$\langle \chi \rangle_a = N\beta p^2 \cos^2\theta \quad .$$

For random crystallites as well as single crystals of Pa3 structure, $\cos^2\theta$ averages to 1/3 (see Eq.12), hence

$$\langle \chi \rangle_a = (1/3)N\beta p^2 \quad .$$

For case (b) described above, $P = Np\langle \cos\theta \rangle$, the bracket denoting the thermal average. The relative probability of finding P di-

rected into a given element of solid angle $d\Omega$ is, by Boltzmann distribution, proportional to $\exp(-\beta\varepsilon)$. Hence in case (b), the average χ can be written as (Kit71, Rei65)

$$\langle \chi \rangle_b = (Np/E) \frac{\int \exp(-\beta\varepsilon)\cos\theta \, d\Omega}{\int \exp(-\beta\varepsilon) \, d\Omega}$$

$$= (Np/E) \frac{\int 2\pi \sin\theta\cos\theta \exp(\beta Ep\cos\theta) \, d\theta}{\int 2\pi \sin\theta \exp(\beta Ep\cos\theta) \, d\theta}$$

$$= (Np/E) \, L(q) \quad ,$$

where $q = \beta Ep$ and $L(q)$ is the famous Langevin function. At high temperature ($q \ll 1$), $L(q) \simeq (q/3) = (\beta Ep/3)$, and hence

$$\langle \chi \rangle_b = (1/3)N\beta p^2 \quad .$$

For rotations along the body diagonals in case (c), an approach similar to the derivation in case (a) can be applied (the difference is that now we have eight possible states instead of two). It can be shown that the average susceptibility for case (c) in the high temperature limit is

$$\langle \chi \rangle_c = N\beta p^2 \langle \cos^2\theta \rangle \quad .$$

We have shown in Eq.(12) that for rapid reorientations between the body diagonals, the average of $\cos^2\theta = 1/3$, and hence the three cases yield a common result. That is, $\langle \chi \rangle_a = \langle \chi \rangle_b = \langle \chi \rangle_c = (1/3)N\beta p^2$. We can thus conclude from the result derived above: given that head-tail flips occur rapidly in α-CO above 45 K, one cannot observe by dielectric means jump rotations between the body diagonals or even free rotations.

Chapter IV

EXPERIMENTS AND PULSE TECHNIQUES

4.1 EXPERIMENTS

We found in the last chapter that the chemical shift anisotropy and intermolecular dipole-dipole interactions are separately sensitive to reorientations and translations, respectively. Furthermore, since either interaction can be made to dominate the spectrum by appropriate choice of the field and C^{13} enrichment, the rotations and the translations can be measured separately.

Experimentally, the rotations were detected at high field and low C^{13} concentration through the modulation of chemical shift anisotropy; spin echoes and stimulated echoes were used. The translational jumps modulate the dipolar interactions and were studied at low field and high C^{13} enrichment using line narrowing and $T_{1\rho}$ measurements. The pulse sequences used in the experiments and the related phenomena will be described in this chapter.

The description of the sample gas bottles, sample mixing, and sample handling are all described in Chapter II. In the α-CO experiments, the high and low C^{13} concentration samples used have concentrations of 90% and 10%, respectively. In the CO_2 experiments, 99% and 15% C^{13}-enriched samples were used.

4.2 HIGH FIELD EXPERIMENTS

Experiments at high field were all done at a resonance frequency of 14.7 MHz, corresponding to a field strength H_0 ~ 13.7 kilogauss. This is the maximum field of our high impedance electromagnet.

4.2.1 Lineshape Study

The C^{13} lineshapes at high field were investigated on samples of both high and low C^{13} concentrations. The lineshapes were obtained by fourier transforming the free induction decay (FID) signals and/or spin echoes (Hah50). The FIDs were produced by a $180^{\circ}_{x/-}$ (blinking) - τ - 90°_{y} pulse sequence. The subscript 'x' means rotation about that axis, and '-' implies no rotation and '$\bar{x}$' means rotation in the opposite sense.

Take the external magnetic field H_0 along the + z direction and consider a reference frame rotating at angular velocity ω_0 about the z-axis with respect to the laboratory frame (Sli80, Abr83). In the rotating frame, before applying the 90° pulse, the net magnetization lies along either the +z or -z direction. The net magnetization arises from the external field H_0 which establishes a net spin population at thermal equilibrium; the ratio of the spin populations is given by the Boltzmann distribution. The 'blinking' 180° pulse before the 90° pulse alternates on and off producing a change in the direction of the magnetization from -z to +x direction. The 90°_{y} pulse rotates the net magnetization about the y-axis. Immediately after the 90° pulse is turned off, since the magnetic field felt by the spins is different in different portions of the sample due to the chemical shift anisotropy, the

spin isochromats (spins in portion of sample precessing at the same frequency) precess and soon get out of phase, causing the decay of the FID signal. The blinking 180^0 pulse alternates the direction of the magnetization and hence the sign of the FID signals, allowing for add/subtract averaging and elimination of coherent noise such as electrical and acoustic ringing (which are not sensitive to the initial inversion pulse). The fixed spacing τ between the two pulses (typically ~ 3×10^{-2} s) is chosen so that $\tau << T_1$. Typically, 40 FID signals were averaged to increase the signal-to-noise ratio (S/N), each sequence spaced by ~ $5T_1$ allowing the magnetization to reach its equilibrium value.

At high field, the chemical shift anisotropy (CSA) interaction is the dominant source of line broadening. In the low temperature (rigid lattice) limit, one expects from the axial symmetry of the CO and CO_2 molecules that the NMR spectrum should be a uniaxial powder pattern. The shift anisotropy $\Delta\sigma$ (Eq.5) can be easily determined from the NMR spectrum. By comparing the spectra from the low and high C^{13}-enriched samples, one can observe the broadening of the line by the increased C^{13} dipolar coupling as the C^{13} concentration is increased.

Furthermore, if the rotational jump rate $\omega_j = 1/\tau_j$ is faster than the static (rigid lattice) powder pattern linewidth $\Delta\omega_{RL}$, one expects to observe line narrowing (Sli80, Abr83, Pop59) due to motional averaging. Usually, the line narrowing occurs near the melting point and the linewidth measurement in the line narrowing region can be used to derive the jump rate.

Experimentally, the high field lineshape study in α-CO indicates that the jump rate ω_j is too slow to cause line narrowing. That is, α-CO is always in the slow jump regime, $\omega_j < \Delta\omega_{RL}$. Line narrowing was observed for the CO_2 lines at high field near the melting point, in contrast to α-CO which transforms to the plastic β-phase before narrowing can occur.

4.2.2 Spin Echo: T_2 Measurements

A $90^\circ_{x/\bar{x}} - \tau - 180^\circ_y$ pulse sequence (Hahn50) was used to measure the relaxation time T_2 in the low C^{13} concentration samples. The phase of the two pulses are 90° out-of-phase and the phase of the first pulse was alternated ($x/\bar{x}$) for signal averaging purposes.

Initially, the magnetization is fully recovered and aligned along the z-axis, parallel to the external field H_0. In the rotating frame, during the 90° pulse (at t = 0), the magnetization processes an angle of 90° about H_1 in the x-y plane. During the time interval τ, the spin isochromats dephase due to the chemical shift anisotropy. The 180° pulse (at t = τ) rotates the spin isochromats in the x-y plane by 180° about the y-axis. The spin isochromats continue to precess at the same rate and rephase to form a net magnetization after a time (τ) equal to the time spent dephasing. That is, the isochromats refocus to give a spin echo (usually called "Hahn echo") at time 2τ. The spin echo is symmetric about the position at t = 2τ, consisting of two FIDs back-to-back. Hence, the spin echo can also be used to determine lineshape provided that the pulse spacing $\tau << T_2$. The transverse relaxation time T_2 was determined from the dependence of the echo amplitude on the echo time 2τ, given by

$$M(2\tau) = M_0 \exp(-2\tau/T_2) ,$$

where M_0 is the magnetization at thermal equilibrium. Typically, 20 spin echoes were averaged for a given value of τ to increase the signal-to-noise ratio.

In the slow jump limit (Sil80, Pop59) where the jump rate ω_j is too small to cause line narrowing ($\omega_j \leq \Delta\omega_{RL}$, $\Delta\omega_{RL}$ is the powder pattern linewidth), only those spins which have remained at the same frequency (and hence orientation) during the entire 2τ interval will contribute to the spin echo. Those spins that change frequency get out of phase and hence will not contribute to the echo. Thus, rotational jumps cause the echo amplitude to decay as $\exp(-2\tau/\tau_j)$, where τ_j is the mean time between rotational jumps. The dipolar interaction between the C^{13} spins is a like-spin term (Eq.9) and is not refocused by the 180^0 pulse. Consequently, the echo envelope will also decay due to the dipolar effects (temperature independent) with an approximately Gaussian envelope (Abr83). The reason for not studying the high C^{13}-enriched sample with spin echoes is because the dipolar interaction is so large that the echo envelope is almost always determined by the spin-spin processes instead of the molecular jumps.

4.2.3 Stimulated Echo Measurements

A $90^0_{y/\bar{y}} - \tau - 90^0_y - T - 90^0_y$ pulse sequence was used to generate stimulated echoes (Hah50) at high field and low C^{13} concentration. Data were obtained by averaging typically 20 echoes at each T value. The advantage of the stimulated echo is that slower

motion can be studied than with the conventional two-pulse spin echo technique.

After the first 90° pulse, the spin isochromats precess at different rates in the xy-plane (rotating frame) due to chemical shift anisotropy. Assuming the initial frequency of the isochromats is ω_i as given by Eq.(5), the x and y components of the magnetization are given by the Bloch equations (Blo46) as:

$$M_x(\tau) = - M_0 \cos(\omega_i \tau) \exp(- \tau/T_2)$$
$$M_y(\tau) = M_0 \sin(\omega_i \tau) \exp(- \tau/T_2) \quad .$$

For the pulse spacing $\tau << \tau_j$ (as always used here, $\tau = 6 \times 10^{-4}$ s and $\tau_j \geq 5 \times 10^{-3}$ s) the orientation of the molecules and hence the frequency of the isochromats may be considered to be unchanged during the interval from $t = 0$ to τ. The second 90° pulse stores the x-component of the magnetization along the $\pm$ z-axis; the z-component of the magnetization right after the second 90° pulse is given by

$$M_z(\tau) = - M_0 \cos(\omega_i \tau) \exp(- \tau/T_2).$$

The first two pulses constitute the " preparation" part of the pulse sequence.

During the waiting time T after the second pulse, molecular rotations may occur. Hence we assume that the isochromat has some new frequency $\omega_f = \omega_i + \Delta\omega$ during the interval from $t = \tau+T$ to $2\tau+T$ (where the stimulated echo occurs).
After the third 90° pulse, the z-component of the magnetization will be brought into the x-y plane again and precess accordingly. The planar

components of the magnetization at $t > \tau + T'$ can be expressed as

$$M_+(t') = M_x(t') + iM_y(t')$$
$$= -M_0 \cos(\omega_i\tau)\left[\cos(\omega_f t') + i \sin(\omega_f t')\right] \times \exp\{-(t'+\tau)/T_2\} \quad ,$$

where $t' = t-(\tau+T')$. In the case when $\omega_f = \omega_i$, the x-component of the magnetization can be written as

$$M_x(t'=\tau) = - M_0 \cos^2(\omega_i\tau) \exp(-2\tau/T_2) \quad .$$

Averaging over all ω_i and assuming that τ is long compared to the reciprocal linewidth T_2^*, we find that $M_x(t'=\tau) = -(1/2)M_0$. Hence a stimulated echo appears at time τ after the 90^0 pulse.

An isochromat that changes its frequency by $\Delta\omega = \omega_f - \omega_i$ will contribute to the echo an amount

$$M_x(t'=\tau) = - M_0 \cos(\omega_i\tau)\cos(\omega_f\tau)$$
$$= - (M_0/2)\left[\cos(\Delta\omega\tau) - \cos[(\omega_i+\omega_f)\tau]\right]. \qquad (16)$$

Again assuming that $\tau >> T_2^*$ and averaging over all isochromats, we find $\langle\cos[(\omega_i+\omega_f)\tau]\rangle$ in Eq.(16) vanishes; the bracket $\langle \ \rangle$ has been used to denote the average. Hence, the amplitude of the stimulated echo is just

$$M_x(t'=\tau) = -(1/2)M_0 \langle\cos(\Delta\omega\tau)\rangle \quad . \qquad (17)$$

From Eq.(17) we see that for large $\Delta\omega\tau$, $M_x(t'=\tau) = 0$ and for small $\Delta\omega\tau$ it is $-(1/2)M_0$. Therefore by varying τ, one controls the size of frequency jump $\Delta\omega$ to which this technique is sensitive.

Because the orientation information is stored as z magnetization during the waiting interval T', it relaxes in a time of order T_1. This is in contrast to the conventional spin echo which involves planar magnetization that relaxes with time constant T_2. In our system T_1 is typically 50 to 100 s, much longer than the longest value of T' used (4 s). Futhermore, spectral diffusion will serve to destroy the stimulated echo. For the samples under investigation, since each crystallite generally contains just four well-separated NMR frequencies (four molecular orientations each corresponding to a body diagonal of the Pa3 structure) and since the dipolar interactions are small (low C^{13} enrichment), the spectral diffusion is expected to be slow. In other words, spectral transfer is slow because neighboring isochromats generally belong to entirely different crystallites. Because T_1 and spectral diffusion are so slow, very slow rotations may be studied with stimulated echoes.

The effect of the rotational jumps on the stimulated echo may be readily seen. A given molecule can jump between just four different orientations and hence four different NMR frequencies. Provided that $\tau >> T_2^*$, an isochromat that has a net frequency change during the interval T' will not contribute to the stimulated echo; this is because $\langle \cos(\Delta\omega\tau) \rangle$ from Eq.(17) will be zero for such isochromats. That is, only those spins with no net frequency (or net orientation) change will contribute to the stimulated echo. Hence, the stimulated echo amplitude is proportional to the fraction of molecules that are in the same orientation at the end of the T' interval as at the start. Clearly, there is a 1/4 probability of a molecule returning to

its initial orientation, even at $\tau = \infty$. We expect the stimulated echo envelope to decay exponentially with a time constant of order τ_j (the mean jump time), but to a baseline of 1/4 of the $\tau = 0$ echo amplitude. As shown in Appendix C, the echo envelope is

$$A(\tau) = \frac{3}{4} \exp\left(-\frac{4}{3}\omega_j \tau\right) + \frac{1}{4} . \qquad (18)$$

Hence the mean jump time τ_j is just 4/3 of the characteristic decay time of the exponential part.

Stimulated echoes have been used by others to observe or search for slow rotations (Spi80, Sol82, Yu83). The stimulated-echo pulse sequence is also the basis of many two-dimensional Fourier-transform techniques in NMR (Jee79). The fundamental concept is information storage along the $\pm$ z axis.

4.3 LOW FIELD EXPERIMENTS

Experiments at low field were done at 1.256 MHz, corresponding to a magnetic field strength of 1.2 kilo-gauss. Both line narrowing and T_{1D} experiments were performed with highly C^{13}-enriched samples.

4.3.1 Line Narrowing

The lineshapes at low field were obtained by Fourier transforming 40 free induction decay signals or magic echoes (Bow82). At low field and high C^{13} concentration, the dipolar interaction is expected to be larger than the chemical shift anisotropy. At high temperature where line narrowing ($\omega_j \geq \Delta\omega_{RL}$) (Sli80, Pop59) was observed,

the lineshapes were obtained using FIDs generated by the same pulse sequence described earlier. In the rigid lattice (low temperature) limit, in order to obtain a reliable second moment (M_2) measurement from the lineshape, a $\tau_x - \tau_{\bar{x}} - 90^o_y$ magic echo pulse sequence (Bow82, Kuh84) was used to overcome the receiver blocking (deadtime) which obscured the initial part of the decay signal and hence affected the measurement of moments. A blinking 180^o pulse was placed in front of the magic echo pulse sequence for signal averaging purposes.

The sophisticated spin dynamics associated with magic-echo formation have been developed and well described by Rhim, Pines, and Waugh (Rhi70). The formation of the magic echo using a long rf pulse (typically many times the 180^o pulse length) whose pulse length is much greater than T_2 violates the spin-temperature (Red55, Sli61, Jee68) hypothesis (but works all the same). During the long rf pulse, the dipolar system behaves as though the dipolar Hamiltonian were reversed in sign (Rhi70). Thus, the system appears to develop backwards in time; subsequent forward time evolution after the pulse yields the magic echo. The echo has minimal lineshape distortion and gives a better determination of M_2 than other techniques (such as the solid echo technique described in Ref. Man65 and Pow63).

Dipolar lineshapes have been widely used in NMR to determine the structure and motion of solids. However, it is not yet possible to determine (i.e. theoretically) the explicit form of the shape function $F(\omega)$ in solids, due to the many-body nature of the spin interactions. The shape of the resonance curve (i.e. the frequency spectrum) can be related to the properties of the spin system by Van Vleck's method of

moments (Van48, Abr83). The second moment M_2 is probably the most important and valuable among moments because it may be experimentally determined with accuracy and may be calculated easily. The Van Vleck calculation of the second moment for the like-spin dipolar interaction in a powder has been given by Eq.(11). Experimentally, the second moment can be obtained by intergrating the frequency spectrum $F(\omega)$ using the definition of M_2 (Abr83):

$$M_2 = \left[\int (\omega - \omega_0)^2 F(\omega) d\omega\right] \Big/ \int F(\omega) d\omega \quad . \tag{19}$$

Alternatively, the second moment can also be determined from the time domain free induction decay $G(t)$, where $G(t)$ is the Fourier transform of $F(\omega)$. As given by Ref.Abr83, M_2 is

$$M_2 = \frac{(-1)}{G(0)} \left| \frac{d^2 G(t)}{dt^2} \right|_{t=0} \quad . \tag{20}$$

where $G(0)$ is the initial ($t = 0$) height of the FID. The experimental second moment determined using both time and frequency domain approaches will be compared to the theoretical calculation in Chapter V.

The onset of line narrowing occurs when $\omega_j \simeq \Delta\omega_{RL}$ (Sli80, Pop59), where $\Delta\omega_{RL}$ is the rigid lattice linewidth at HWHM (half width at half maximum). Thus, the observation of line narrowing can be used to calculate the jump rate $\omega_j = 1/\tau_j$ at one temperature.

4.3.2 Jeener Echo: T_{1D} Measurements

The Jeener-Broekaert pulse sequence, $90^{o}_{x/\bar{x}} - \tau - 45^{o}_{y} - T - 45^{o}_{y}$ (Jee67), was used to measure the relaxation time T_{1D} of the C^{13} spins in the dipolar ordered state (And62). Data were obtained by averaging 20 to 40 Jeener echoes at each T value.

Initially, before applying the 90^{o} pulse, the nuclear spin system is in thermal equilibrium with the lattice. The first two pulses in the pulse sequence transform the initial Zeeman order into dipolar order (And62). Jeener and Broekaert showed (Jee67) that a maximum efficiency of transfer from the Zeeman order to dipolar order can be obtained with a $\pi/2$ phase shift between the first (90^{o}) pulse and the second pulse (45^{o}) separated by a time of order T_2. During the waiting interval T, molecules may execute translational jumps and hence destroy the dipolar order (since the local dipolar fields are spacially random) (Sli64). The third pulse (phase is arbitary) transforms the remaining dipolar order back into Zeeman order: a "Jeener echo" (or "dipolar FID") is observed.

For system with a single dipolar spin temperature (Sli80, Abr83), one expects the Jeener echo to decay exponentially as a function of T with time constant T_{1D} approximately equal to τ_j. The experimental T_{1D} results will be compared to the τ_j data from the stimulated echo measurements using Eq.(15); details will be seen in Chapter V.

Chapter V

EXPERIMENTAL RESULTS AND DISCUSSION

5.1 HIGH FIELD EXPERIMENTS

At high field (14.7 MHz), chemical shift anisotropy (CSA) is the dominant source of line-broadening. The rotational motion was detected through the modulation of chemical shift anisotropy using spin echoes and stimulated echoes. The pulse sequences and pulse techniques used to generate echoes have been described in Chapter IV.

5.1.1 Carbon Monoxide Results

The C^{13} line shapes in both 90% and 10% enriched CO samples were investigated at high field (14.7 MHz) and are shown in Figs.7(a) and 7(b). The lines are approximately uniaxial powder patterns, as expected. By comparing the high- and low-concentration spectra in Figs.7(a) and 7(b), we notice that the C^{13} dipolar couplings which increase with increasing C^{13} concentrations only serve to broaden the sharp features of the powder pattern; the overall powder linewidth did not change indicating that CSA is indeed dominating the spectra. The shift anisotropy ($\Delta\sigma$) is 5200 $\pm$ 200 Hz (350 $\pm$ 15 ppm) near 50 K, in good agreement with a previous C^{13} NMR measurement (335 $\pm$ 20 ppm at 46 K) by Gibson and co-workers (Gib77). They observed a slight temperature dependence (365 $\pm$ 20 ppm at 4.2 K) of the shift anisotropy due to motional averaging caused by rapid librations.

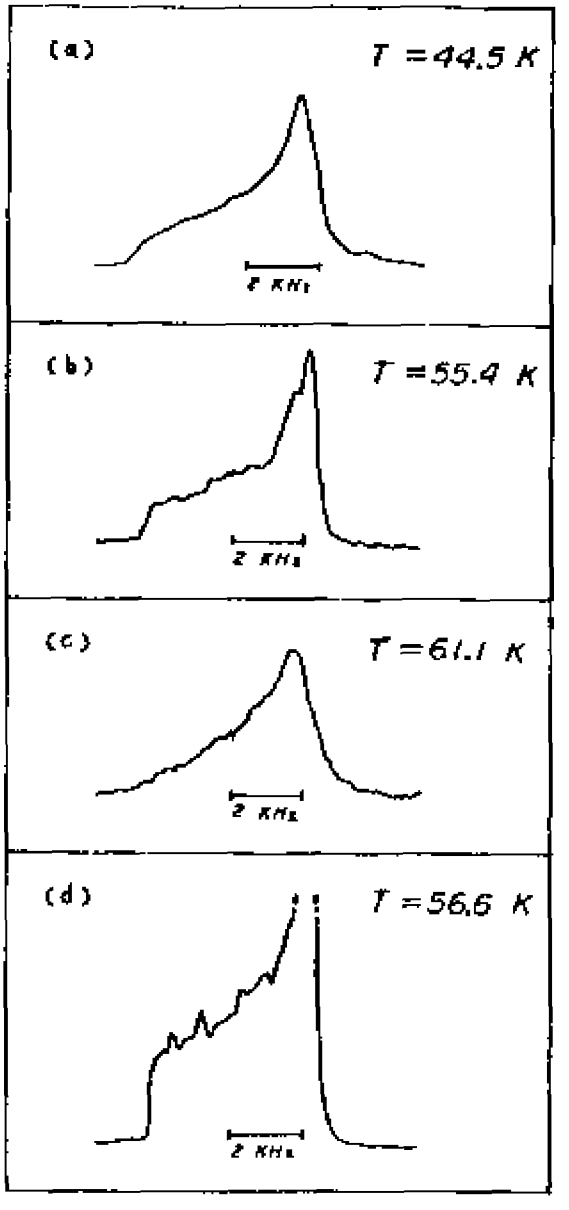

Figure 7: C^{13} NMR spectra of solid α-CO at high field (14.7 MHz). (a), 90% C^{13}; (b), 10% C^{13}; note the broadening produced by the dipolar couplings at high concentration. Broadening due to rotational jumps is evident in (c), 10% C^{13} at 61.1 K. Spectrum (d) of high S/N (700 averages) shows non-randomness of crystallite orientations as bumps on resonance.

Line shapes at high field were often noticeably different from the expected uniaxial powder pattern (Eq.8); Gibson and co-workers also observed (Gib77) similar lineshapes which deviate from theoretical curves. The NMR spectrum in Fig.7(d) is the result of averging 700 echoes; the extremely high S/N ratio is indicated by the lack of any apparent noise on the baseline. Hence the bumps on the resonance curve itself are not noise, but reflect the lack of perfect randomness of crystallite orientations in the sample. The occurence of such lines is seemingly related to how the sample is prepared. The α-CO samples were formed from β-CO (hcp structure) which is (similar to β-N_2 (Dov84)) a rapidly annealing material. The hcp and Pa3 crystal structures are related; the relation between the crystal orientations at the hcp-Pa3 phase transition of H_2 has been discussed (Har83). It seems likely that a single crystal or a sample of just a few crystallites of β-CO should not give rise to a true polycrystalline powder of α-CO. We did succeed, seemingly by accident, in growing some good powders of α-CO; the NMR spectra of these samples agree well with the theoretical curve.

If the rotational jump rate ω_J were faster than the rigid lattice powder pattern linewidth $\Delta\omega_{RL}$, line narrowing would be observed (Abr83). The spectrum in Fig.7(c) was obtained from a 10% C^{13}-enriched sample quite near the α-β phase transition ($T_{\alpha\beta}$ = 61.55 K). Although this line is not narrower overall (compare with Fig.7(b)), the sharp features of the powder pattern have been considerably broadened. In the language of chemical exchange (Sli80, Pop59), this behavior indicates that the system is always in the slow-exchange

limit ($\omega_j < \Delta\omega_{RL}$). Hence for α-CO, the jump rate is never sufficiently fast to cause line narrowing ($\omega_j \gtrsim \Delta\omega_{RL}$) below Tαβ at high field.

The relaxation time T_2 was determined from the dependence of spin echo height on the echo time (2τ, see spin echo pulse sequence in Chapter IV) in a 10% C^{13}-enriched CO sample. As described in Chapter IV, in the slow jump (exchange) limit, only those spins which have remained at the same orientation during the entire 2τ interval can contribute to the spin echo. Hence, rotational jumps cause the echo amplitude to decay as $\exp(-2\tau/\tau_j)$, where τ_j is the mean time between orientational jumps and $\omega_j = 1/\tau_j$ is the jump rate.

Experimentally, at high temperatures the echo envelopes decay exponentially and are temperature dependent. At lower temperature ($T \lesssim 57$ K), the envelopes are nearly Gaussian and are temperature independent, as expected from the effect of dipolar interaction (Abr83). The echo envelopes of solid α-CO as a function of the echo time 2τ are shown in Fig.8 at several different temperatures. The dashed line in Fig.8 indicates $M(2\tau)/M(0) = \exp(-2\tau/T_2) = 1/e$. That is, points where the echo envelope intercept the dashed line give the value of T_2 (along the horizontal axis).

All of the T_2 values were obtained using the exponential decay form: $M(2\tau) = M(0)\cdot\exp(-2\tau/T_2)$, even at low temperatures where the echo envelopes are approximately Gaussian. The decay times T_2 so determined are shown in Fig.9 as a function of reciprocal temperature. Clearly, at high enough temperatures (near Tαβ) the T_2 values reflect rotational jumps and should be equal to τ_j. At low temperatures

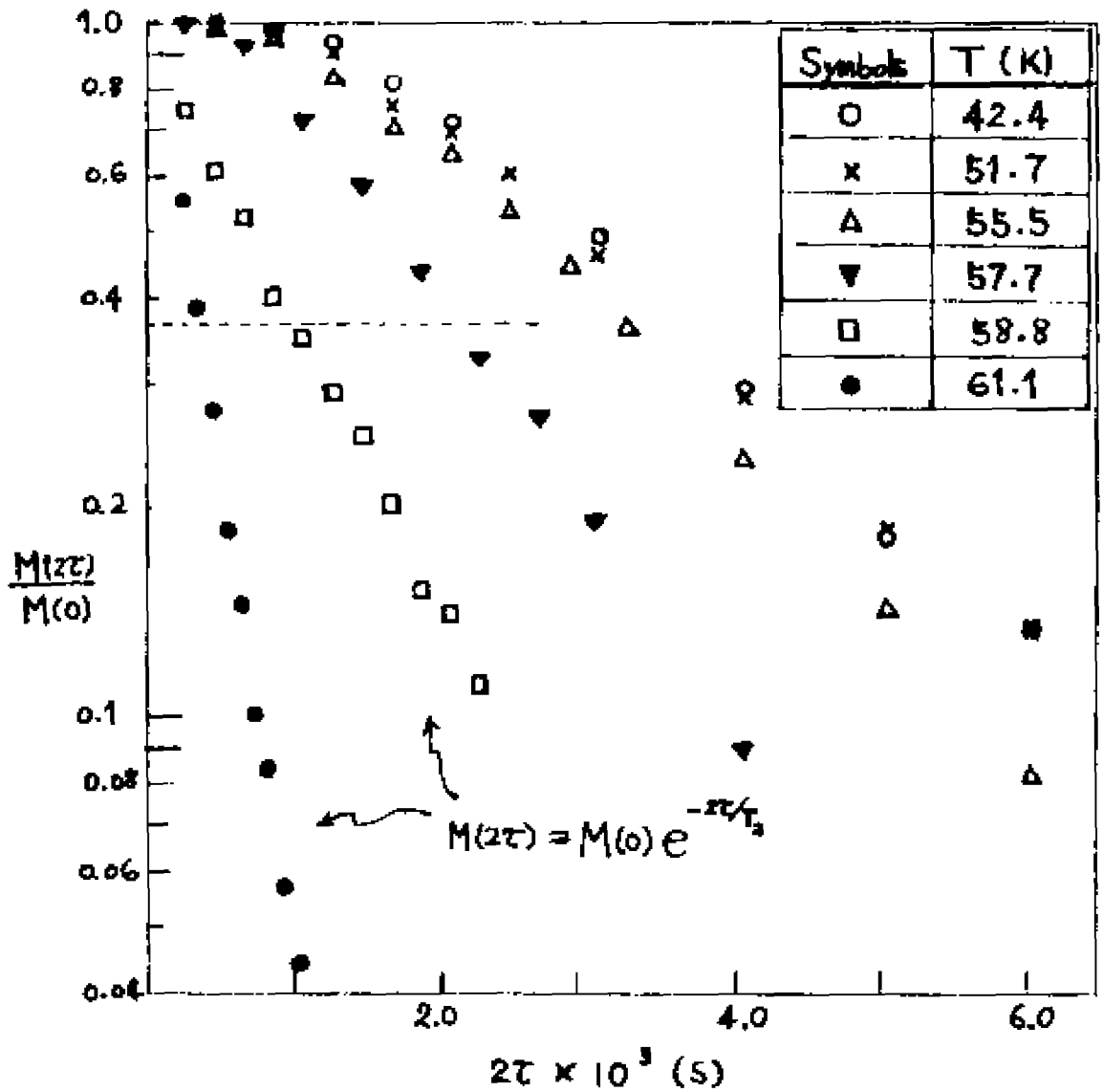

Figure 8: A semi-log plot of high field spin echo envelopes of α-CO at different temperatures. At high T, the echo envelopes are T dependent; they decay exponentially and reflect rotational jumps. At lower T, the envelopes are nearly Gaussian and T independent due to dipolar couplings. The dashed line indicates 1/e of the exponential decay. Similar behavior is also seen in solid CO_2 echo envelopes.

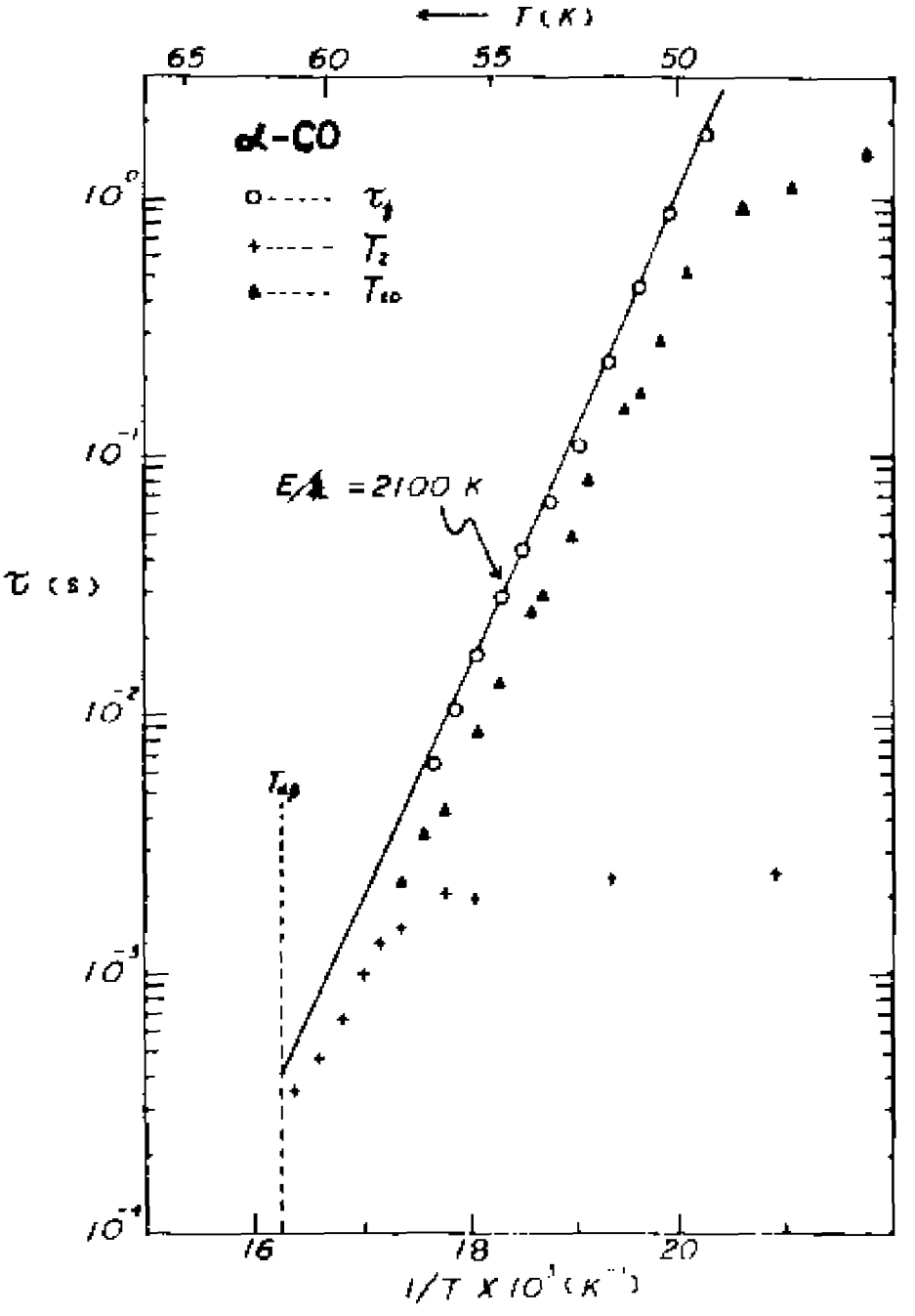

Figure 9: Spin relaxation times closely related to τ_j as a function of reciprocal temperature (semi-log plot). The T_2 from spin echoes (+), τ_j from stimulated echoes (O) and T_{1D} from J-B sequence at low field (Δ) are shown. The stimulated echo values yield τ_j directly. The straight line fit is the activated rate expression (Eq.21), the activation parameters are given in the text.

(T < 57 K) the T_2 values are temperature independent; T_2 is a measure only of the dipolar interactions.

The sample (10% C^{13}) used in the spin echo experiments was also used for the stimulated echo experiments. The advantage of studying stimulated echoes is that slower τ_j can be measured than with conventional spin echo techniques. The pulse sequence and the effect of rotations on the stimulated echo have been presented in Chapter IV. Specifically, for the rotations between the four body diagonals of a Pa3 solid, the stimulated echo envelope should decay exponentially with a time constant of order τ_j, but to a baseline of 1/4 (Eq.18).

Fig.10 shows a typical stimulated echo envelope of solid α-CO; the echo envelope have been scaled so that $A(\tau=0) = 1$. The data points clearly show the expected decay and the baseline; the relative amplitude of the baseline in this example is 0.28. All of the stimulated-echo envelopes examined gave baselines values between 0.25 and 0.30. Using Eq.(18), one obtains the mean jump time τ_j by plotting $A(\tau)-(1/4)A(\tau=0)$ as a function of τ on a semilog graph paper; τ_j is related to the characteristic decay time τ^* by $\tau_j = (4/3)\tau^*$.

The observed values of τ_j from stimulated echoes are shown in Fig.9. They agree reasonably well with the τ_j data obtained from ordinary spin echoes, but extend to motions as slow as $\tau_j = 2$ s. The direction of the offset (factor of ~ 2) between the τ_j data from the stimulated echo and ordinary spin echo can be explained by the dipolar damping of the ordinary echoes. However, quantitative agreement cannot be reached. The straight line in Fig.9 indicates a fit of the stimulat-

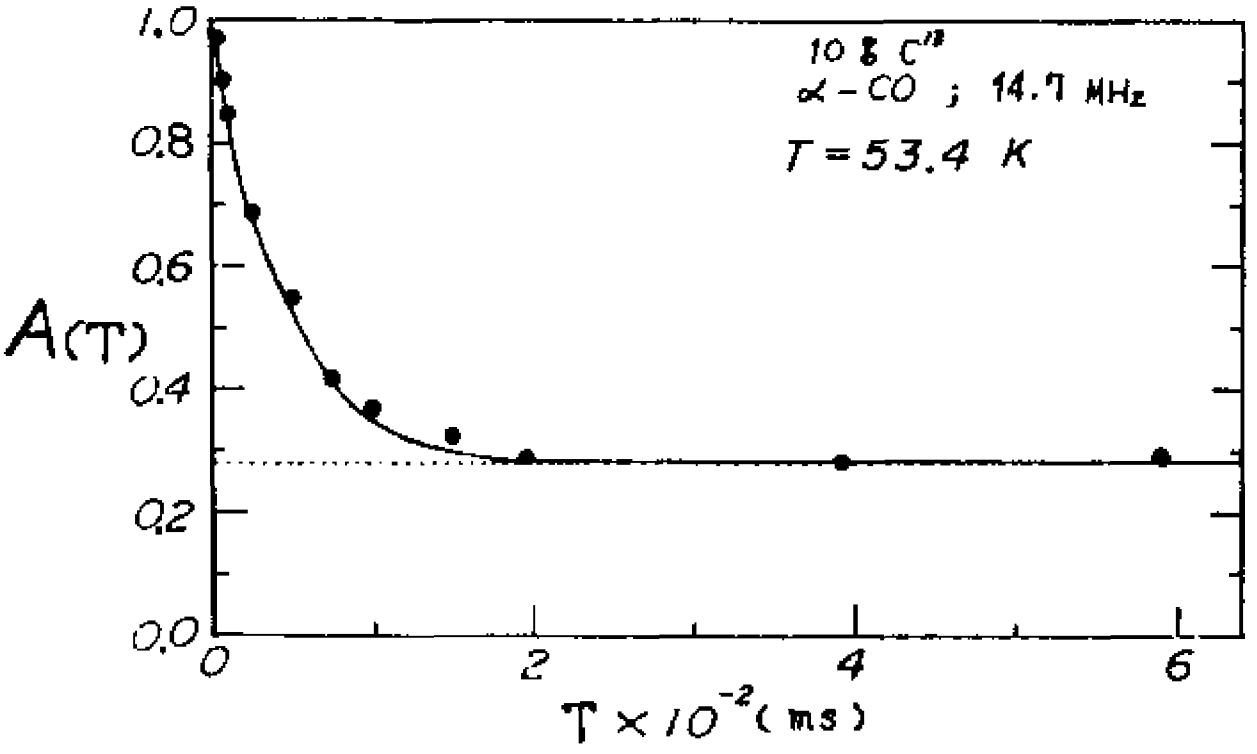

Figure 10: Typical stimulated-echo envelope as a function of waiting inteval τ. The exponential decay to a non-zero baseline (Eq.18) is evident. Similar stimulated-echo envelopes were also seen in CO_2 solid.

ed echo data over three decades to the thermal activation expression (or Arrhenius equation) given by

$$\omega_j = 1/\tau_j = \omega_0 \exp(-E_a/kT). \qquad (21)$$

The activation energy E_a/k is found to be 2100 K and the frequency prefactor is $\omega_0 = 2 \times 10^{18}\ s^{-1}$.

5.1.2 Carbon Dioxide Results

The C^{13} line shapes of solid CO_2 at high field have been investigated in both 15% and 99% C^{13} enriched samples. Samples were prepared in a special way (see Chapter II) to form poly-crystalline powder. The resonance lines of 99% and 15% samples are shown in Figs.11(a) and 11(b). Below 200 K, the resonance lines are uniaxial powder patterns with a shift anisotropy of 4780 $\pm$ 200 Hz (325 $\pm$ 15 ppm). The shift anisotropy reported here agrees very well with a reported 318 $\pm$ 18 ppm anisotropy for $C^{13}O_2$ adsorbed onto sodium mordenite at 30^0 C (Sef78). The spectrum in Fig.11(a) indicates rounding of the sharp features of the powder pattern due to C^{13} dipolar couplings (compare with Fig.11(b)). The shape of the resonances indicates that at high field CSA is the dominant source of broadening.

As temperature is increased toward the melt (T_m = 216.56 K), the sharp features of the powder pattern become rounded and eventually (above 208 K) the line narrows (Figs.11(b) to 11(c)). As the line narrows, it loses its asymmetric shape. This sequence of rounding and then narrowing is just that expected from the theories of motional averaging, such as chemical exchange broadening/narrowing (Sli80, Pop59). The high

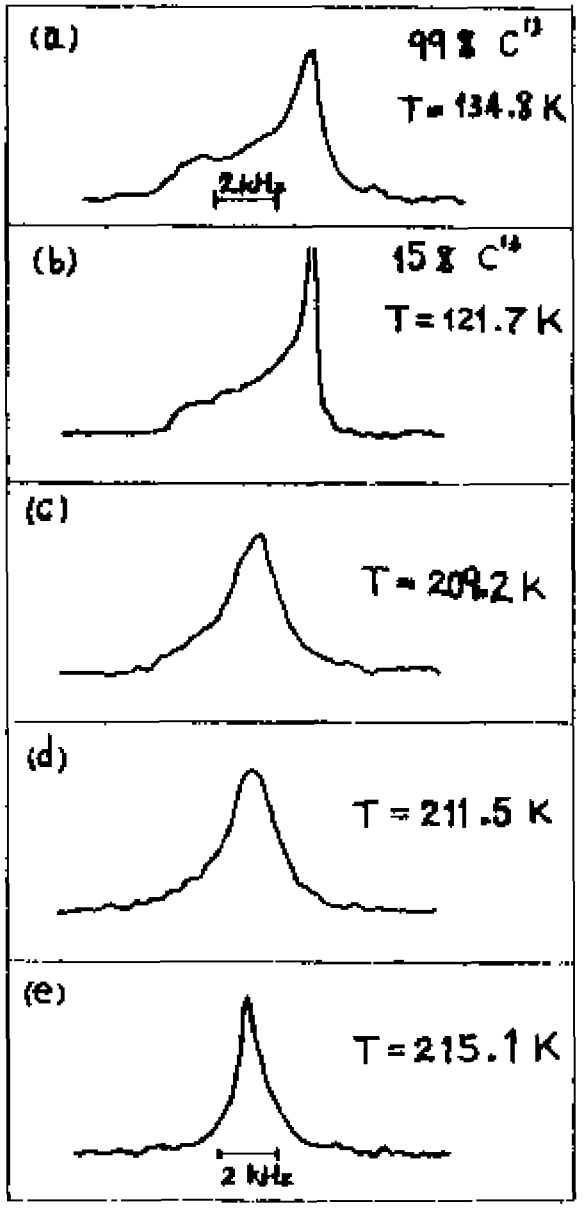

Figure 11: C^{13} NMR spectra of solid CO_2 at high field. Spectrum (a), 99% C^{13} shows broadening due to dipolar interactions by comparing with (b), 15% C^{13}. Spectra (b) to (e), all 15% C^{13}, reveal the sequence of rounding and then narrowing as temperature approaches the melt, as expected for the effect of motional narrowing.

field linewidths (FWHM) as a function of reciprocal temperature are shown in Fig.12 for the 99% as well as 15% samples.

Line narrowing should occur when the rotational jump rate ω_j exceeds the rigid lattice powder pattern linewidth $\Delta\omega_{RL}$ ($2\pi \times 4780$ s^{-1}). The linewidth at high field decreased to about 1000 Hz FWHM near the melt, but the extent of narrowing is too small to allow an activation energy to be determined. The narrowing in solid CO_2 should be contrasted with the behavior in α-CO: the sample transforms to the plastic β-phase before narrowing occurs.

The decay times T_2 for the spin echo experiment (15% C^{13}) are shown in Fig.13 as a function of reciprocal temperature. Experimentally, the spin-echo envelopes are exponential and are temperature dependent at high temperatures. At low temperatures the echo envelopes are nearly Gaussian and are temperature independent. These observations are similar to those of α-CO shown in Fig.8. At high temperatures ($T > 185$ K) the T_2 values (Fig.13) reflect jump rotations, with $T_2 \simeq \tau_j$. Below 185 K, T_2 is only a measure of the dipolar interactions. The minimum in T_2 at 210 K occurs near the onset of motional narrowing, as expected. Hence T_2 is essentially equal to τ_j (a slow motion regime result) only between 185 K and 210 K.

The τ_j measurements were extended to slower motion using stimulated echoes for the same (15%) CO_2 sample. The experimental stimulated-echo envelopes were all observed to decay following Eq.(18) with relative baseline values between 0.2 and 0.4, as expected. The τ_j data from stimulated echoes are shown in Fig.13 as triangles for two 15%-enriched $C^{18}O_2$ samples. The data extend to motions as

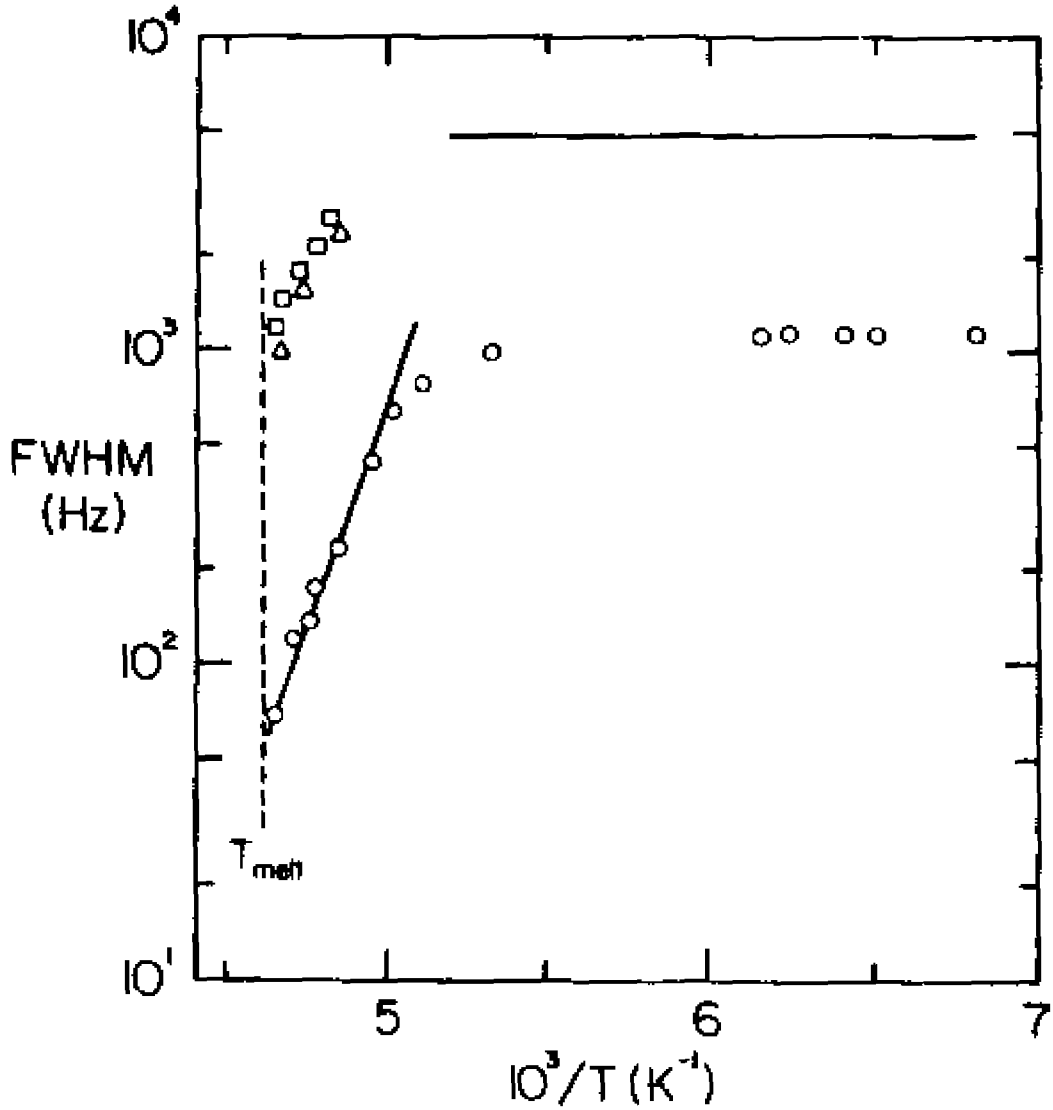

Figure 12: Linewidth FWHM of CO_2 at low field and 99% C^{13} enrichment (circles); this is almost entirely dipolar linewidth. The line through the circles was chosen to have a slope corresponding to the activation energy of 6600 K (determined from data in Fig.13). High field linewidths reflect chemical shift anisotropy and appear as squares (15% C^{13}) and triangles (99%). The horizontal line is the width of the rigid high field powder pattern.

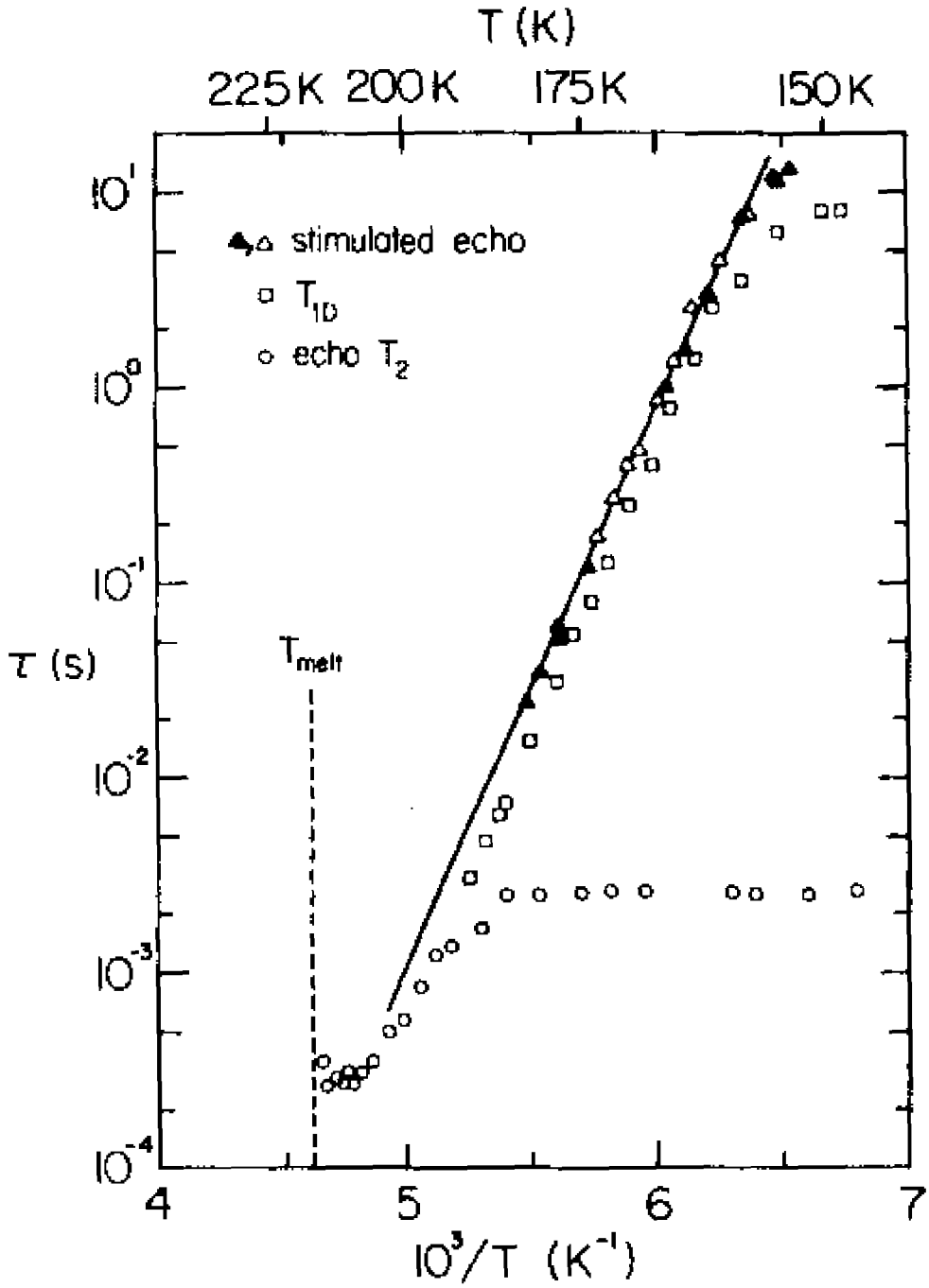

Figure 13: Relaxation times τ in solid CO_2 as functions of reciprocal temperature. The squares are T_{1D} taken at low field and 99% C^{13} enrichment. All the other data are from high field measurements on 1% enriched CO_2. The circles are T_2 from spin echoes; T_2 becomes temperature independent below 185 K because of dipolar coupling. Stimulated echo data from two 1% samples are shown as open and filled triangles. The line drawn is to fit the data and corresponds to an activation energy of 6600 K.

slow as τ_j = 12 s, and agree reasonably well with the T_2 data but with a factor of ~ 2 offset between them. The offset of the τ_j values between the stimulated echo and spin echo measurement was also seen in α-CO, but is not understood. The straight line in Fig.13 indicates a thermally activated fit (Eq.21) of stimulated-echo data over three decades, with activation parameters E_a/k = 6600 ± 300 K and ω_0 = 2 × 10^{17} s^{-1}.

At the lowest temperatures, the stimulated-echo data appear to be leveling off, perhaps because of spectral diffusion. It should be noted that besides molecular rotations, spin-lattice relaxation, spectral diffusion, and the effect of paramagnetic impurities (such as O_2 in the sample) may contribute to the observed decay rate. The level of O_2 doping used here resulted in T_1 ~ 150 s, much longer than the longest τ_j measured (12 s). Hence the leveling off of τ_j data is not due to a T_1 process. For the possibility of diffusion caused by impurities such as O_2, it is believed that impurity concentrations are negligibly small, even though the actual content of O_2 impurity is uncertain. The spectral diffusion is expected to be slow since the dipolar interactions are small (15% C^{13}) and since each crystallite of a Pa3 solid generally contains four well-separated NMR frequencies (Chapter IV).

5.2 LOW FIELD EXPERIMENTS

At low field (1.256 MHz), the C^{13} dipolar interactions are expected to be larger than the CSA. The translational jumps modulate the dipolar interactions and were detected with line narrowing and Slichter-Ailion slow motion (T_{1D}) experiments. The pulse sequences used in the experiments and related phenomena were discussed in Chapter IV.

5.2.1 Carbon Monoxide Results

The C^{13} lineshapes in Fig.14 were obtained by Fourier transforming 40 FIDs from a 90% C^{13}-enriched CO sample. The observed rigid lattice linewidth at 42 K (Fig.14(a)) is 960 Hz FWHM, while the high field anisotropy linewidth (5200 Hz at 14.7 MHz) scales to a 440-Hz width at 1.256 MHz. Since linewidths from different sources typically add as squares, the dipolar interaction is seen to be dominant, as expected. The nearly symmetric shape of the spectrum also indicates that the shift anisotropy is relatively unimportant here.

The Van Vleck expression for the like-spin dipolar part of the second moment M_2 in a powder is given by Eq.(11). For α-CO, the fcc lattice sum $\sum_k r_k^{-6} = 14.45\ d_0^{-6}$, where d_0 is the nearest-neighbor distance of 0.398 nm (Koh60). For C^{13} nuclei of fractional concentration f = 0.9 and using I = 1/2, $\gamma = 6.72 \times 10^3$ rad/gauss.sec, and $\hbar = 1.05 \times 10^{-27}$ erg.sec, the Van Vleck calculation (Eq.11) yields $M_2 = 3.35 \times 10^6$ (rad/sec)^2. The above calculation is based on the simplified assumption that the C^{13} spins are effectively located at the molecular centers. This assumption is correct (Dmi63) in the case of rapid isotropic rotation of the molecules. In α-CO at 42 K, only

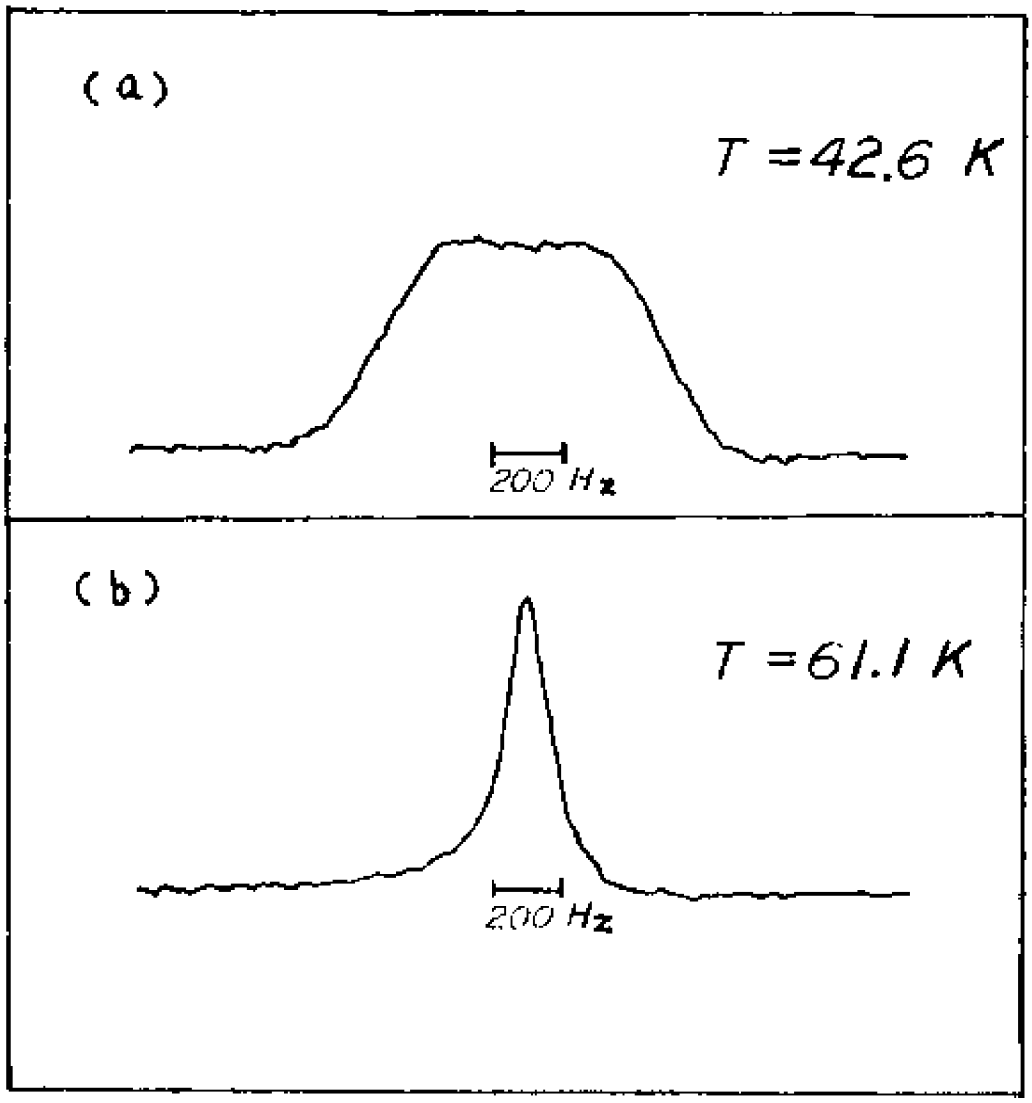

Figure 14: Low field (1.256 MHz) C^{13} spectra of 90% C^{13} enriched α-CO. Spectrum (a) is the rigid lattice spectrum from 42.6 K. Spectrum (b) shows motional narrowing very near Tαβ (61.1 K), demonstrating that translations as well as rotations occur in warm α-CO.

180° flips are occuring rapidly (Nar82), hence the above calculation is only approximate. Furthermore, a computer simulation was performed in which a Gaussian line shape function was convoluted with the shift anisotropy powder pattern; the inclusion of the shift anisotropy according to this simulation increases the calculated M_2 by about 15%.

The experimental second moment was taken from both the frequency spectrum and from the FID, using Eq.(19) and Eq.(20). The two methods gave the same answer: $M_2 = 3.4 \times 10^6$ (rad/sec)^2. This is in reasonable agreement with theory.

The low field, high C^{13} concentration spectrum in α-CO narrows just below Tαβ (61.55 K), as shown in Fig.14(b). The linewidth at 61.1 K is 160 Hz FWHM, smaller than either the dipolar or the CSA contribution to the rigid lattice linewidth. Therefore, the motion is seen to be a translation as well as a rotation.

The onset of motional narrowing should occur when $\tau_j \Delta\omega_{RL} \approx 1$, where $\Delta\omega_{RL}$ is the HWHM linewidth in frequency units. Using $\Delta\omega_{RL} = (1/2) \times 2\pi \times (960\ s^{-1})$, τ_j is 3.3×10^{-4} s at the onset of narrowing. The spectrum of Fig.14(b) is pretty well narrowed, so τ_j is near 3×10^{-4} s at 61 K. This is in reasonable agreement with the value of τ_j extrapolated from the stimulated-echo measurement in Fig.9. From the line narrowing in solid α-CO, it can be concluded that translational jumps occur at approximately the same rate as the rotations studied at high field.

The T_{1D} data in α-CO were obtained by averaging 16 Jeener echoes from a 90% enriched sample at 1.256 MHz and are shown in Fig.9. The rate of translational motion was followed over three decades. The

data above 50 K have the same temperature dependence as the stimulated echo data. This indicates again that in α-CO the translations responsible (primarily) for T_{1D} and the rotations that damp the high field stimulated echoes are parts of the same motion. The reason that T_{1D} becomes temperature independent below 50 K is not known.

The offset between the T_{1D} and stimulated-echo (τ_j) data in Fig.9 can be explained with the strong-collision slow-motion theory of Slichter and Ailion (Sli64, Ail71). Using Eq.(15) and taking $\tau_j = \tau$, one finds experimentally $2(1-p) = 2.0$. The correlation parameter p of vacancy diffusion on an fcc lattice has been calculated theoretically by Ailion and Ho (Ail68); they found $2(1-p) = 1.57$. Wolf included the effects of a " trail of hot spins " left behind by the vacancy and the correlated jumps of neighboring nuclei (Wol74). That is, the vacancy jump time is short compared to the spin internal equilibrium time T_2^* (even though $\tau_j \gg T_2^*$) so that a spin temperature cannot be established between sucessive vacancy jumps nor between those jumps of nuclei which are caused by the same vacancy. Based on the above assumptions, Wolf found $2(1-p) = 0.88$ on an fcc lattice. The reason that the experimental value of $2(1-p)$ deviates from the predicted values may be due to the presence of a non-negligible CSA in the systems reported here.

5.2.2 Carbon Dioxide Results

The line shape of a 99% C^{13}-enriched CO_2 sample has been studied at 1.256 MHz. The spectra shown in Fig.15 are the result of Fourier transforming 100 magic echoes. The rigid lattice linewidth ($T < 185$ K) is 1120 $\pm$ 50 Hz FWHM, and the line (Fig.15(a)) is very nearly

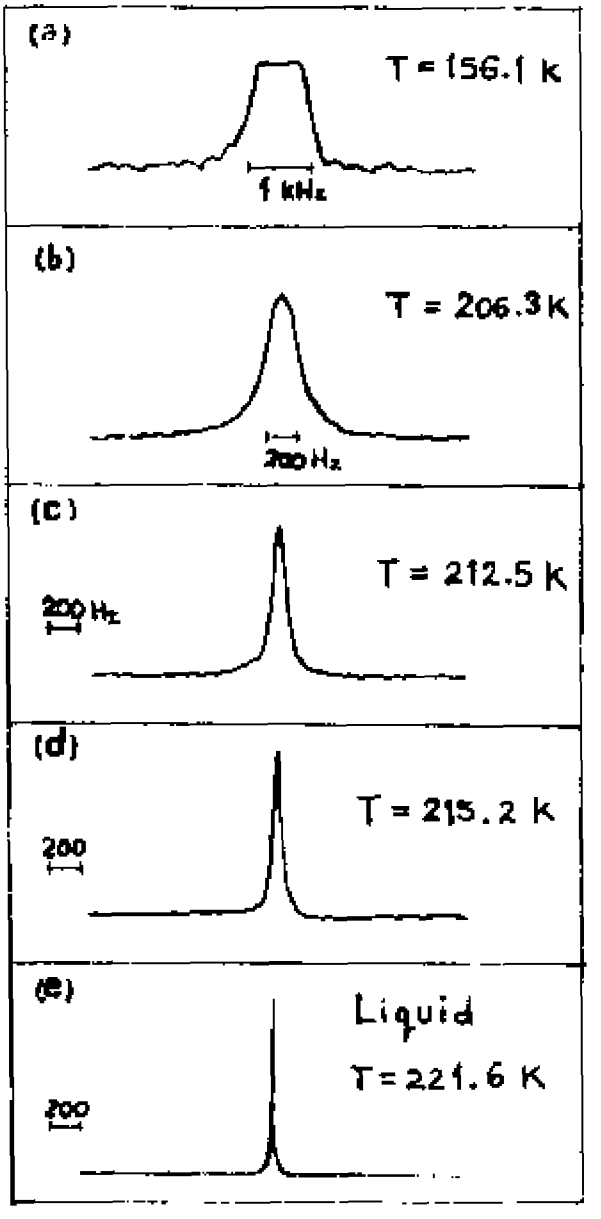

Figure 15: Low field C^{13} spectra of 99% enriched $C^{13}O_2$. Spectrum (a) is the rigid lattice spectrum (1120 Hz FWHM). Spectra (b) to (d) show the effect of line narrowing as the temperature increases. Spectrum (d) is taken very close to the melt (T_m = 216.56 K); the width (68 Hz FWHM) can be compared to the liquid spectrum (e) (20 Hz FWHM) at 221.6 K.

symmetric. At low field (1.256 MHz), the shift anisotropy scales to 410 Hz overall linewidth. Hence the dipolar interactions are seen to be the dominant source of line broadening.

The Van Vleck second moment in this system can be calculated. Again using Eq.(11) with $f = 0.99$, and $d_0 = 0.399$ nm (at 150 K) (Kse34), one obtains $M_2 = 3.63 \times 10^6$ (rad/sec)^2. Experimental second moments from both time domain (Eq.20) and frequency domain (Eq.19) data give $M_2 = (5.0 \pm 0.5) \times 10^6$ (rad/sec)^2. The agreement between the experimental result and the Van Vleck calculation is fair, given that the CSA has been ignored. By including the shift anisotropy the calculated M_2 increases to 4.67×10^6 (rad/sec)^2, according to the computer simulation described earlier.

The experimental line-widths are shown in Fig.12 as circles. The line narrows above 195 K (Fig.15(a) to 15(d)), becoming as narrow as 68 Hz FWHM near the melt ($T_m = 216.56$ K). This is much smaller than either the dipolar contribution or the shift anisotropy contribution to the rigid lattice linewidth. Hence at high temperatures, both rapid translations and rotations occur in CO_2 solid. The linewidth in the liquid phase is 20 Hz FWHM (presumably, all magnet inhomogeneity) at 221.6 K and the line is shown in Fig.15(e) for comparison.

The onset of motional narrowing ($\tau_j^{-1} \approx \Delta\omega_{RL}$, where $\Delta\omega_{RL}$ is the linewidth at HWHM) occurs at ~ 210 K. Using $\Delta\omega_{RL} = (1/2) \times (2\pi \times 1120\ s^{-1})$, τ_j is 2.8×10^{-4} s at the onset of narrowing, in agreement with the value of τ_j extrapolated from the high field stimulated-echo measurement (Fig.13).

The spin-lattice relaxation times (T_{1D}) of the nuclear spin dipolar-ordered state were studied using a 99% enriched sample at low field. Typically 40 Jeener echoes were averaged at each τ values (see section 4.3.2); the T_{1D} results are shown in Fig.13. The rate of motion ($\tau_j \sim T_{1D}$) was followed over three decades. Above 155 K, the temperature dependence of T_{1D} and τ_j from stimulated echoes are the same, indicating that the translations and rotations are two aspects of one combined motion. The temperature independence of T_{1D} below 155 K is not understood: T_1 was typically 150 s, much greater than T_{1D}, and hence T_1 processes can not be the cause.

Similar to that described in α-CO, the T_{1D} data may be treated with SA (strong-collision) slow-motion theory using Eq.(15). The experimental offset between the T_{1D} and stimulated-echo τ_j data indicates $2(1-p) = 1.8$. In α-CO, the quantity $2(1-p) = 2.0$, close to the value found here. The presence of shift anisotropy prevents a comparison of the theoretical $2(1-p)$ values with the experimental data. However, to within a factor of 2 uncertainty in the correct value of $2(1-p)$, the translation and rotation jump rates are seen to be equal. Hence, the combined translational-rotational jumps occur in solid CO_2 as well as in α-CO.

5.3 DISCUSSION

As described in Chapter I, α-CO, α-N_2, CO_2, and N_2O belong to a family of orientationally ordered solids with Pa3 structure and composed of linear molecules. The C^{13} NMR experiments reported here confirmed that the combined translational-rotational jumps occur in solids α-CO and CO_2.

Reorientations in solid N_2O have been studied dielectrically (Nar82); the reorientation rate ω_R was found to follow the activated rate expression (Eq.21) with activation energy E_a/k = 6020 K and ω_0 = 5.6×10^{19} s^{-1}. Time-domain dielectric experiments have extended the data to lower temperature (Fic83); the activated expression holds from the melt (ω_R = 3×10^5 s^{-1}) to near 120 K where ω_R = 10^{-2} s^{-1}. This uncommonly large range of ω_R values lends extra strength to the unusual activation parameters (especially ω_0).

N^{14} NMR experiments (Dov84) similar to those reported here indicate that molecular reorientation through an angle substantially different from 180° occurs in solid N_2O. This reorientation cannot be the head-tail flips which occur in solid α-CO, but are probably due to the combined translational-rotational jumps. The reorientation rate from the N^{14} NMR data has the same activation energy as does the dielectric relaxation data (Nar82), but the NMR rate is ~ 10 times slower. In any event, it appears that the motion seen in N_2O is the same as that seen in this report for α-CO and CO_2.

Solid α-N_2, the other member of the Pa3 family, exists at much lower temperature ($T_{\alpha\beta}$ = 35.61 K); hence translational diffusion is likely to be too slow to be detected. This is the reason why α-N_2 has not been studied.

5.3.1 Combined Jumps In Other O. O. Solids

The combined translation-rotations have been found in other orientationally ordered (O. O.) solids, such as ammonia (NH_3) and benzene (C_6H_6). Solid NH_3 is cubic in structure (belongs to space

group $P2_13$) at low pressure (Mil84). The molecule has a tetrahedral shape with its 3-fold symmetry axis oriented along a body diagonal of the cube. Hence in solid NH_3, translation is accompanied by a reorientation of the molecular 3-fold axis. Early proton $T_1\rho$ measurements (O'Re70), fitted with Torrey's theory of relaxation by translational diffusion (Tor53), found that the diffusion jump rate is thermally activated and gave $E_a/k = 4727$ K with $\omega_0 = 1 \times 10^{15}$ s^{-1}. Recent NMR experiments in this laboratory (Dov85) measured the combined translation-rotations in solid NH_3 at three different pressures (0, 2, and 4 kbar) using proton T_{1D} as a probe. Thermally activated jump diffusion gave $E_a/k = 5870$ K and $\omega_0 = 5 \times 10^{17}$ s^{-1} at ambient pressure. Jump diffusion has also been studied in solid ND_3 (Dov85) with stimulated echoes using the technique of deuteron spin alignment (Spi80); the relaxation data gave an activation energy nearly equal to that found in NH_3.

Solid benzene ($T_m = 278.6$ K), another O. O. molecular solid, has orthorhombic crystal structure (space group Pbca) (Cox58). The crystal consists of four sub-lattices; hence when a given molecule diffuses, it moves to a new sub-lattice and reorients accordingly. Self-diffusion in benzene reveals a dramatic difference in diffusion data using different measuring techniques. The first diffusion measurement of benzene was reported by Fox and Sherwood using the radio-tracer method (Fox71); they found thermally activated diffusion with $E_a/k = 11600$ K and $\omega_0 = 2.8 \times 10^{24} s^{-1}$. Later, the diffusion in benzene was measured using proton NMR T_{1D} and $T_1\rho$ as probes (Ste69, Noa75). Using Torrey's diffusion model (Tor53), the NMR data indicate that the activa-

tion energy is roughly the same but the diffusion coefficient is about four order of magnitude smaller than the tracer result. Recently, a proton decoupled C^{13} NMR experiment in this laboratory (Gul85) reexamined self-diffusion in solid benzene. Using techniques similar to those reported here, the activation parameters (E_a/k = 11420 K and ω_0 = 4.2 $\times$ 10^{20} s^{-1}) of diffusion were determined, in agreement with the previous proton NMR measurements (Nos75).

It is interesting that the combined translation-rotations which occur in these orientationally ordered molecular solids all show high activation parameters. Particularly, they all have unusually high frequency pre-factors ω_0. In this report, the jump rates ω_j of solid α-CO and CO_2 were fit only to stimulated echo data. We believe this procedure reduces the possibility of obtaining incorrect ω_0 values. For example, if ω_j data from the stimulated echoes and from line narrowing were used, the data would clearly extend over a wider range of temperature. But the activation energy obtained would be sensitive to any possible multiplicative factors in the interpretation of each kind of data. Resulting small errors in the activation energies, while not serious in themselves, would produce large errors in the frequency prefactors. However, the ω_0 values obtained using only stimulated echo data are almost insensitive to any numerical factors (such as 4/3 in Eq.(18)). Hence, the ω_0 values should be correct even if the detailed model of the motion is uncertain.

As in rare gas solids or in metals, one expects these orientationally ordered molecular solids (α-CO, α-N_2, CO_2, N_2O, NH_3, and C_6H_6) to obey some type of scaling relations between the

activation parameters and thermodynamic quantities. This will be discussed further in the next section.

5.3.2 Diffusion In Molecular Crystals

Diffusion in molecular crystals, though not as well studied as that in metals, has progressed with the developement of experimental techniques (such as the NMR slow motion techniques used here). While the defect structure of the molecular crystalline state is not yet well understood, a general description of diffusion via the vacancy mechanism has been formed. Diffusion via thermally generated vacancies is common among molecular solids (She79, Che79) and has been considered as the most likely means for molecular migration. However, among diffusion studies in molecular solids, diffusion in orientationally ordered (O. O.) crystals has scarcely been reported. The most commonly studied materials are those molecular solids in their plastic (orientationally disordered) phases; various attempts to correlate the activation energy and diffusion coefficients with thermodynamic parameters have been made (Che79). A similar approach will be made on the O. O. solids mentioned earlier, namely, α-CO, CO_2, N_2O, NH_4, and benzene. For the molecular solids under investigation, the anisotropic (i.e. non-spherical) intermolecular potential of the molecules cannot be described by a single " strength " parameter. Hence, a strict law of " corresponding states " (originally developed for a set of materials such as rare gas solids that differ only by certain scaling factors) are not expected to hold. Nevertheless, because of the similarities of these solids (especially the family of Pa3 solids), certain scaling relations are expected to apply, although with only limited accuracy.

In metals and rare gas solids, scaling relations between the activation energy (E_a) for diffusion and thermodynamic quantities (such as the melting temperature T_m, melting enthalpy L_m, and sublimation enthalpy L_s) have been tried. General reviews of similar approaches on many molecular solids (mostly plastic crystals) have been presented by Sherwood (She69) and Chereau and Strange (Che79). In closed packed metals, a correlation of E_a/T_m = 134 J/mole K (Che79) is found to be obeyed reasonably well. Furthermore, an emprical relationship E_a/L_m = 16.5 is also in good agreement with observations in metals. In molecular solids, however, neither of the above relations are found to apply except for some molecules with low melting points (Che79). Since a vacancy induced diffusion mechanism is the most likely way for molecular migration, the activation energy E_a for diffusion will be closely related to the lattice energy. The activation energy is the sum of two contributions, the energy for formation E_f and the energy for migration E_m of the diffusing vacancy. For molecular solids as a group, E_f is believed approximately equal to the lattice energy E_l and is of the same order of magnitude but larger than E_m (She69). That is, for vacancy diffusion $E_a = E_f + E_m < 2E_l$. The lattice energy is approximately equal to the latent heat of sublimation L_s so that $E_a \sim 2L_s$.

The activation energies for the combined translation-rotation jumps are compared to the latent heat of sublimation for α-CO, CO_2, N_2O, NH_3, and benzene. As shown in Table III, the ratios are all very nearly equal to 2.15 ($\pm$ 0.03) except for NH_3. The agreement in the O. O. molecular solids α-CO, CO_2, N_2O, and C_6H_6 suggests that the same mechanism is responsible for diffusion in the four

TABLE III

Comparison of Activation Energies and Sublimation Enthalpies and List of Frequency Prefactors in alpha-CO, CO_2, N_2O, NH_3, and Benzene.

	α-CO	CO_2	N_2O	NH_3	C_6H_6
T_{triple} (K)	68.09(a)	216.56(b)	182.26(c)	195.36(d)	278.67(e)
Tαβ (K)	61.55(a)	-----	-----	-----	-----
E_a/k (K)	2100(f)	6600(g)	6020(h)	5870(i)	11420(j)
L_s/k (K)	989(k)	3039(l)	2782(m)	3494(n)	5425(p)
E_a/L_s	2.12	2.17	2.16	1.68	2.11
a (Å)	3.98(q)	3.91(q)	3.99(q)	3.59(r)	7.88(s)
ω_0 (s^{-1})	2×10^{18}(f)	2×10^{17}(g)	6×10^{19}(h)	5×10^{17}(i)	4×10^{20}(j)
D_0 (cm^2/s)	5×10^{2}	5×10^{1}	2×10^{4}	1×10^{2}	1×10^{6}

(a) Ref.: Cla32. (b) Ref.: New62. (c) Ref.: Blu35.
(d) Ref.: Ove37. (e) Ref.: And53.
(f) Ref.: Liu84a, this report.
(g) Ref.: Liu84b, this report.
(h) Ref.: Nar82. (i) Ref.: Dov85. (j) Ref.: Gul85.
(k) Ref.: Cla32, at Tαβ.
(l) Ref.: Gia37, at normal sublimation point (194.7 K).
(m) Ref.: Blu35, at triple point.
(n) Ref.: Ove37, at triple point.
(p) Ref.: Che79. (q) Ref.: Mel64. (r) Ref.: Leh65.
(s) Ref.: Noa75.

materials. The fact that the E_a/L_s ratio for NH_3 (1.68) is much less than the others reflects that NH_3 is not a Van der Waals solids, but has important hydrogen bonding (Dov85).

Diffusion in the rare gas solids is known to proceed via monovacancies (Cha77). The ratio E_a/L_s is 1.9 in the classical rare gas solids (Hen72, Cow76) Ar, Kr, and Xe. Neon should not be included in this comparison because of its substantial quantum effects (Hen72). Diffusion in the plastic (β) phase of CO also is described by this value of the ratio (Fuk77). In fact, in many molecular solids, diffusion data indicate that the ratio E_a/L_s is approximately 2.0; it varies from one material to another in the range 1.6 to 2.5 (Cho79, Sho69). In short, the value of the ratio in the Pa3 solids is typical of molecular solids and the rare gas solids.

Heat capacity measurements of CO_2 and N_2O show a concave upwards rise at high temperatures (Man71, Ats74). This rise has been interpreted as orginating in orientational defects in the Pa3 structure with energy E^*. In CO_2, E^*/k is found to be 1000 $\pm$ 100 K (Man71), while in N_2O the energy is 1200 K (Ats74). The agreement of these independent analyses is striking. The heat capacity analyses indicate that ~ 2% of the molecules have defective orientations near the melt. The energies E^* are much smaller than the activation energies listed in Table III. It is not clear whether orientational defects are involved in the combined translation-rotation jumps. It should be noted that such heat capacity analyses are quite uncertain (Cha77) because of the difficulty in estimating the background (no defects) heat capacity.

5.3.3 High Frequency Prefactors

As described earlier, combined translation-rotations occur in O. O. molecular solids α-CO, CO_2, N_2O, NH_3, and benzene. A surprising result in all these O. O. solids is the high value of the preexponential frequency ω_0 (Table III). For comparison with the data, the experimental ω_0 values have been converted to diffusion pre-factors (D_0) using the Einstein relation (She63, Che79):

$$D_0 = (1/6)\, a^2 \omega_0 \ , \tag{22}$$

where a is the nearest neighbor distance. The D_0 values so determined are shown in Table III.

The simplest theories (Che79, She63) predict

$$D_0 = (1/6)\, z \gamma_D a^2 \ , \tag{23}$$

where z is the number of nearest neighbors (z=12 for fcc lattice) and γ_D is the Debye frequency. Probably the best experimental D_0 value in the classical rare gas solids is from Xe^{133} NMR data (Yen63, Sir77), $D_0 = 10\ cm^2/s$. For α-CO, CO_2, N_2O, NH_3, benzene, and rare gases Ar, Kr, and Xe, Eq.(23) predicts $D_0 = (7 \pm 3) \times 10^{-3}\ cm^2/s$. Clearly, for all O. O. solids listed in Table III and for Xe, the experimental D_0 is three to nine order of magnitude faster than that of the simple prediction by Eq.(23).

The multiplicative offset between the experimental D_0 (from Eq.(22)) and the D_0 predicted from Eq.(23) is commonly treated as arising from the activation entropy of diffusion S_a, a sum of a defect formation entropy S_f and a defect migration S_m. The full expression for

diffusion coefficient D via vacancy is usually expressed as (She63, Che79):

$$D = D_0 \exp(-E_a/kT) \quad ,$$

$$\text{where} \quad D_0 = (1/6)\, f z \gamma_v a^2 \exp(S_a/k) \quad . \qquad (24)$$

The value γ_v is the jump attempt frequency and f is a fractional factor accounting for the effect of correlated jumps. Since there is no method for the direct determination of γ_v, it is often taken as being equal to the Debye frequency γ_D (Eq.23). The effects of correlated jumps only changes the ω_0 values by a factor of order 2 (since $1/2 < f \leq 1$) and has been neglected in the calculation of D_0 in Table III. It should be noted that the ω_0 values determined using Eq.(21) are only accurate to a factor of 10, hence the effect of correlated jumps does not matter. In the rare gas solids, it has been calculated (Cha77, Gly67) that $S_f/k \sim 2$ and $S_m/k \sim 8$. Hence, the rare gas D_0 values are in reasonable accord with the theory given by Eq.(24). Unfortunately, no theoretical calculation is available for the O. O. molecular solids listed in Table III; it is not clear whether a calculation similar to that of rare gases can explain the large ω_0 and D_0 values in these solids.

Chapter VI

CONCLUSIONS

The C^{13} NMR studies reported here confirm that orientationally ordered molecular solids α-CO and CO_2 perform translational-rotational jumps. This motion has also been found in the orientationally ordered solids N_2O, NH_3, and benzene.

The translation and rotation jump rates have been determined independently using samples of various C^{13} enrichment with different magnetic fields and NMR techniques. The rate of translation was obtained with highly C^{13} enriched samples at low field through the modulation of intermolecular dipole-dipole interactions; line narrowing and SA slow motion techniques were used. The rotation jump rate was studied at high field and small C^{13} concentration through the modulation of the chemical shift anisotropy; spin echoes and stimulated echoes were used. The rates of translation and rotation so determined are found to be equal, indicating the occurence of the combined jumping in these orientationally ordered solids, as expected.

The rate of the combined jumps in α-CO and CO_2 were both followed over three decades and the jump rates in both materials are found to be thermally activated. The activation parameters were determined to be E_a/k = 2100 K and $\omega_0 = 2 \times 10^{18}\ s^{-1}$ for α-CO, and E_a/k = 6600 K and $\omega_0 = 2 \times 10^{17}\ s^{-1}$ for CO_2. The unusually large frequency prefactors ω_0 of α-CO and CO_2 have also been observed for

the same motion in N_2O, NH_3, and benzene. However, the high prefactors are not understood. The activation energies for the combined motion in the family of linear molecular solids with Pa3 structure (α-CO, CO_2, and N_2O) and benzene agree well when scaled by their latent heats of sublimation. The ratios E_a/L_s are all found to be 2.15 $\pm$ 0.03; this agreement suggests that the same mechanism is responsible for diffusion throughout the family of Pa3 solids and benzene. However, detailed behavior of diffusion among these orientationally ordered solids remains a challenge to future diffusion studies.

The shift anisotropies ($\Delta\sigma$) are determined to be 350 $\pm$ 15 ppm for α-CO and 325 $\pm$ 15 ppm for CO_2, both in good agreement with previous NMR measurements.

Appendix A

TYPICAL TEMPERATURE CONTROLLER SETTINGS FOR THE MEDIUM (LN_2) TEMPERATURE EXPERIMENTS

	TEMPERATURE CONTROLLER SETTINGS**		
TEMPERATURE (K)	RESISTANCE(Ω)	POWER*	GAIN*
78	20.0	0.3	6.0
90	26.5	0.5	7.0
100	32.0	0.5	7.0
105	35.5	0.5	8.0
120	35.0	1.0	2.0
130	40.0	1.5	2.0
140	45.0	3.0	2.0
145	47.5	4.0	3.0
150	50.0	4.0	3.0
156	55.0	4.0	3.0
165	57.0	5.0	6.0
170	59.0	5.0	6.0
175	61.0	5.0	6.0
181	64.0	5.0	6.0
188	66.0	5.5	6.0
193	70.0	5.5	6.0
202	72.0	6.0	8.0
212	76.0	7.0	9.0
223	81.0	10.0	9.0
250	91.0	11.0	13.0

**Under normal operating conditions:

1. Temperature controller mode selection on 'copper', and the dewar thermometer is PRT (100 Ω at room T).
2. The inner well exhaust valve is off.
3. Control external N_2 gas flow so that the inner well pressure is ~ 3 psig and the flow bore flow reads ~ 5 SCFH.
4. The vacuum pump should be kept on and the N_2 cryo-pump valve is open.

*Normalized scale readings, directly taken from the temperature controller.

Appendix B

TYPICAL TEMPERATURE CONTROLLER SETTINGS FOR THE LOW (LHE) TEMPERATURE EXPERIMENTS

	TEMPERATURE CONTROLLER SETTING*			VAPOR FLOW RATE**	
T (K)	RESISTANCE	POWER	GAIN	FLOW BORE	INNER WELL EXHAUST
4.6	---	---	---	3.5	---
5.6	---	---	---	2.0	0.3
7.1	---	---	---	0.65	0.75
9.0	---	---	---	0.35	1.2
11.2	---	---	---	0.2	1.2
12.7	295	7.0L	1.5	0.8	1.5
14.7	269	9.5L	2.0	1.0	1.4
17.6	240	9.5L	2.0	1.0	1.4
20.4	205	15.0L	4.0	1.0	1.4
25.0	191	1.0H	9.0	1.0	1.4
29.0	180	1.0H	9.0	1.0	1.4
34.3	172	1.0H	11.5	1.0	1.4
39.5	162	1.0H	11.5	1.0	1.4
43.7	155.5	1.0H	11.5	1.0	1.4
47.9	150	1.0H	11.5	1.0	1.4
50.0	148.5	1.0H	11.5	1.0	1.4
52.7	138	1.5H	11.5	1.0	1.4
56.8	140	1.5H	11.5	1.0	1.4
60.8	138	1.5H	12.0	1.0	1.4
72.8	128	3.0H	13.0	1.0	1.4
77.4	128	4.0H	14.0	1.0	1.4

*Under normal operating conditions:
1. The inner well pressure is ~ 0.5 psig, and
the flow bore ~ 1.0 SCFH
the inner well exhaust ~ 1.5 SCFH.
2. The vacuum valve on the dewar is closed.
3. Use Lake Shore carbon-in-glass thermal resistor.

**Vapor flow rate is in unit of SCFH.

NOTE: a). For T < 10 K, the temperature controller is turned off, and the temperature is controlled by the vapor flow only.

b). The power and the gain setting are directly taken from the back of the temperature controller. The 'L' and 'H' are stand for the low and high power output switch on the controller, respectively.

Appendix C

DERIVATION OF THE STIMULATED ECHO ENVELOPE

Consider a single molecule in a Pa3 structured solid which can jump between four different orientations corresponding to the four body diagonals of the cube. Assume that the given molecule has a probability ω_j per unit time of going to any of the other orientations. And, take $P_m(t)$ as the probability of finding the given molecule in orientation m (m = 1, 2, 3, or 4 which correspond to the four body diagonals shown in Figure 1) and W_{mn} as the conditional probability per unit time of the molecule initially in orientation m going to orientation n. One obtains from a master rate equation

$$P_n(t+\delta t)-P_n(t) = \sum_{m(\neq n)} W_{nm}P_m(t)\delta t - \sum_{m(\neq n)} W_{mn}P_n(t)\delta t \quad . \qquad (C1)$$

where W_{mn} and W_{nm} are equal by detailed balance since all four orientations are equally likely in equilibrium. Because any given molecule is surrounded by four members of each of the other three sublattices, W_{mn} and W_{nn} are both equal to $\omega_j/3$ for $m \neq n$. Together with the condition $\sum P_m = 1$, the derivative form of Eq.(C1) is

$$\frac{dP_n(t)}{dt} = \frac{\omega_j}{3}\left[1-4P_n(t)\right], \quad n = 1,2,3,4. \qquad (C2)$$

Taking the molecule initially (t = 0) in orientation m (this is indicated by superscript m), the solution of Eq.(C2) is

$$P_n^m(t) = \frac{3}{4}\exp[-(4/3)\omega_j t] + \frac{1}{4} \quad ,$$

$$P_n^m(t) = \frac{(-1)}{4}\exp[-(4/3)\omega_j t] + \frac{1}{4} \quad , \; n \neq m \quad . \qquad (C3)$$

Here, $P_n^m(t)$ is the conditional probability that given a molecule is in orientation m at time 0, it is in orientation n at time t.

The stimulated-echo amplitude is directly propotional to a single-particle, two-time orientation correlation function; as given by Eq.(16) this is

$$A(T) = \langle \cos(\omega_i \tau)\cos(\omega_f \tau) \rangle \quad .$$

Here the bracket denotes the average over all isochromats and, hence, crystallite orientations. At time $T = 0$, the initial orientation m is equally likely to be any of the four possible. Thus the above can be written as

$$A(T) = \frac{1}{4}\sum_{m,n} P_n^m(T)\langle \cos(\omega_m \tau)\cos(\omega_n \tau) \rangle \quad .$$

The averaging over all isochromats involves only the cosine term. The approximation $\tau >> T_2^*$ allows us to write

$$\langle \cos(\omega_m \tau)\cos(\omega_n \tau) \rangle = (1/2)\delta_{mn} \quad .$$

Hence the observed stimulated-echo amplitude will be

$$2A(T) = \frac{3}{4}\exp[-(4/3)\omega_j T] + \frac{1}{4} \quad , \qquad (C4)$$

where the solution for $P_n^m(\tau)$ of Eq.(C3) has been used. Hence $A(\tau)$ decays exponentially with time constant $(3/4)\tau_j$ to a relative baseline of 1/4.

REFERENCES

Abr83 A. Abragam, The Principles of Nuclear Magnetism (Oxford, 1983), paperback ed..

Ail68 D.C. Allion and P.-P. Ho, Phys. Rev., 168, 662 (1968).

Ail71 D.C. Allion, in Advances in Magnetic Resonance, edited by J.S. Waugh (Academic Press, 1971), Vol. 5.

And53 E.R. Andrew and R.G. Eades, Proc. Roy. Soc., A218, 537 (1953).

And62 A.G. Anderson and S.R. Hartmann, Phys. Rev., 128, 2023 (1962).

Ata74 T. Atake and H. Chihara, Bull. Chem. Soc. Japan, 47, 2126 (1974).

Ata76 T. Atake, H. Suga, and H. Chihara, Chem. Lett. (Japan), 1976, 567.

Blo46 F. Bloch, Phys. Rev., 70, 460 (1946).

Blo48 N. Bloembergen, E.M. Purcell, and R.V. Pound, Phys. Rev., 73, 679 (1948).

Blo55 N. Bloembergen and T.J. Rowland, Phys. Rev., 97, 1679 (1955); also see Acta Metall., 1, 731 (1953).

Blu35 R.W. Blue and W.F. Giauque, J. Amer. Chem. Soc., 57, 991 (1935).

Bow82 R.C. Bowman and W.-K. Rhim, J. Magn. Reson., 49, 93 (1982).

Bro84 J. Brookeman, A. Rigamonti, and N.S. Sullivan, Ferroelectrics, 54, 53 (1984).

Cha77 A.V. Chadwick and H.R. Glyde, in Rare Gas Solids, edited by M.L. Klein and J.A. Venables (Academic, N.Y. 1977), Vol. 2.

Che79 J.M. Cherean and J.H. Strange, Phys. Rep., 53, 1 (1979).

Cla32 J.O. Clayton and W.F. Giauque, J. Amer. Chem. Soc., 54, 2610 (1932).

Con77 M.S. Conradi, Rev. Sci. Instrum., 48, 359 (1977).

Cow76 D.F. Cowgill and R.E. Norberg, Phys. Rev., B13, 2773 (1976).

Cox58 E.G. Cox, Rev. Mod. Phys., 30, 159 (1958).

Cro76 V.E. Cross, R.K. Hester and J.S. Waugh, Rev. Sci. Instrum., 47, 1486 (1976).

Din62 F. Din, editor, Thermodynamic Functions of Gases, (Butterworths, London, 1962), Vol. 3.

Dmi63 L.V. Dmitrieva and V.V. Moskalev, Fiz. Tverd. Tela (Leningrad), 5, 2230 (1963); or see Sov. Phys.- Solid State, 5, 1623 (1964).

Dov83 M.A. Doverspike, work done in this laboratory (unpublished).

Dov84 M.A. Doverspike and M.S. Conradi, Phys. Rev., B30, 4905 (1984).

Dov85 M.A. Doverspike, S.-B. Lin, P. Ennis, T. Johnson, M.S. Conradi, K. Luszczynski, and R.E. Norberg, submitted for pulication (1985).

Ell71 J.D. Ellett,Jr., M.G. Gibby, U. Haeberlen, L.M. Huber, M. Mehring, A. Pines, and J.S. Waugh, in Advances in Magnetic Resonance, edited by J.S. Waugh (Academic Press, 1971), Vol. 5.

Fic83 D.J. Ficenec, B. A. Thesis, The College of William and Mary (1983).

Fox71 R. Fox and J.N. Sherwood, Trans. Faraday Soc., 67, 3364 (1971).

Fuk77 E. Fukushima, A.A.V. Gibson, and T.A. Scott, J. Chem. Phys., 66, 4811 (1977).

Fuk79 E. Fukushima, A.A.V. Gibson, and T.A. Scott, J. Chem. Phys., 71, 1531 (1979).

Fuk81 E. Fukushima and S.B.W. Roeder, Experimental Pulse NMR : A Nuts and Bolts Approach (Addison-Wesley, 1981).

Gia33 W.F. Giauque and J.O. Clayton, J. Amer. Chem. Soc., 55, 4875 (1933).

Gia37 W.F. Giauque and C.J. Egan, J. Chem. Phys., 5, 45 (1937).

Gib77 A.A.V. Gibson, T.A. Scott, and E. Fukushima, J. Magn. Reson., 27, 29 (1977).

Gly67 H.R. Glyde, Rev. Mod. Phys., 39, 373 (1967).

Gul85 T. Gullion and M.S. Conradi, submitted for publication (1985).

Hae76 U. Haeberlen, in High-Resolution NMR in Solids, Advances in Magnetic Resonance, edited by J.S. Waugh (Academic, 1976), supplement 1.

Hah50 E.L. Hahn, Phys. Rev., 80, 580 (1950).

Har62 S.R. Hartmann and E.L. Hahn, Phys. Rev., 128, 2042 (1962).

Har83 A.B. Harris, S. Washburn, and H. Meyer, J. Low Temp. Phys., 50, 151 (1983).

Hen72 R. Henry and R.E. Norberg, Phys. Rev., B6, 1645 (1972).

Jee67 J. Jeener and P. Broekaert, Phys. Rev., 157, 232 (1967).

Jee68 J. Jeener, in Advances in Magnetic Resonance, edited by J.S. Waugh (Academic Press, N.Y., 1968), Vol. 3.

Jee79 J. Jeener, B.H. Meier, P. Bachmann, and R.R. Ernst, J. Chem. Phys., 71, 4546 (1979).

Jor64 T.H. Jordan, H.W. Smith, W.E. Streib, and W.N. Lipscomb, J. Chem. Phys., 41, 756 (1964).

Kan80 S. Kan, M. Fan, and J. Cortieu, Rev. Sci. Instrum., 51, 887 (1980).

Kee34 W.H. Keesom and J.W.L. Köhler, Physica (Utrecht), 1, 655 (1934).

Kit71 C. Kittel, Introduction to Solid State Physics (John Wiley and Sons, 1971), 4th ed..

Koh60 B.C. Kohin, J. Chem. Phys., 33, 882 (1960).

Kru73 I.N. Krupskii, A.I. Prokhvatilov, A.I. Erenburg, and L.D. Yantsevich, Phys. Stat. Sol., (a) 19, 519 (1973).

Kuh83 P.L. Kuhns, Thesis, The College of William and Mary (1983).

Kuh84 P.L. Kuhns and M.S. Conradi, J. Chem. Phys., 80, 5851 (1984).

Lea62 A.S. Leah, in Thermodynamic Functions of Gases, edited by F. Din (Butterworths, London, 1962), Vol. 1.

Leh65 S.S. Lehrer and C.T. O'Konski, J. Chem. Phys., 43, 1941 (1965).

Li81 F. Li, J.R. Brookeman, A. Rigamonti, and T.A. Scott, J. Chem. Phys., 74, 3120 (1981).

Liu84a S.-B. Liu and M.S. Conradi, Phys. Rev., B30, 24 (1984).

Liu84b S.-B. Liu, M.A. Doverspike, and M.S. Conradi, J. Chem. Phys., 81, 6064 (1984).

Loo66 D.C. Look and I.J. Lowe, J. Chem. Phys., 44, 2995 (1966).

Man65 P. Mansfield, Phys. Rev. 137, A961 (1965).

Man71 V.G. Manzhelii, A.M. Tolkachev, M.I. Bagatskii, and E.I. Voitovich, Phys. Stat. Sol., 44b, 39 (1971).

Meh71 M. Mehring, R.G. Griffin, and J.S. Waugh, J. Chem. Phys. 55, 746 (1971); also see J. Chem. Phys. 57, 2147 (1972).

Meh76 M. Mehring, in High Resolution NMR Spectroscopy in Solids, NMR Basic Principles and Progress, edited by P. Diehl, E. Fluck, and R. Kosfeld (Springer-Verlag, N.Y., 1976), Vol. 11.

Mel64 M.W. Melhuish and R.L. Scott, J. Phys. Chem., 68, 2301 (1964).

Mil69 R.L. Mills and A.F. Schuch, Phys. Rev. Lett., 23, 1154 (1969).

Mil84 R.L. Mills, D.H. Liebenberg, R. LeSar, and Ph. Pruzan, in High Pressure in Science and Technology, edited by C. Homan, R.K. MacCrone, and E. Whalley (North-Holland, N.Y., 1984), Vol. 22, part 2.

Nag60 O. Nagai and T. Nakamura, Prog. Theore. Phys., 24, 432 (1960).

Nar82 K.R. Nary, P.L. Kuhns, and M.S. Conradi, Phys. Rev., B26, 3370 (1982).

New62 D.M. Newitt, M.U. Pai, N.R. Kuloor, and J.A.W. Huggill, in Thermodynamic Functions of Gases, edited by F. Din (Butterworths, London, 1962), Vol. 1.

Nos75 F. Nosek, M. Weithase, and J. Van Schüte, Z. Naturforsch., A30, 1707 (1975).

ORe70 D.E. O'Reilly, E.M. Peterson, and S.R. Lammert, J. Chem. Phys., 52, 1700 (1970); also see D.E. O'Reilly and E.M. Peterson, J. Chem. Phys. 56, 5536 (1972).

Ove37 R. Overstreet and W.F. Giauque, J. Amer. Chem. Soc. 59, 254 (1937).

Par78 N.G. Parsonage and L.A.K. Staveley, Disorder in Crystals (Clarendon Press, Oxford, 1978).

Pop59 J.A. Pople, W.G. Schneider, and H.J. Bernstein, High-Resolution Nuclear Magnetic Resonance (McGraw-Hill, 1959).

Pow63 J.G. Powles and J.H. Strange, Proc. Phys. Soc., 82, 6 (1963).

Rab75 The Radio Amateur's Handbook, R.M. Wilby editor (American Radio Relay League, Inc. Newington, Conn., 1975), 52th ed..

Rei71 J.C. Reich and R.L. Mills, J. Chem. Phys., 55, 1811 (1971).

Ram50 N.F. Ramsey, Phys. Rev., 78, 699 (1950); also Phys. Rev., 86, 243 (1952).

Red55 A.G. Redfield, Phys. Rev., 98, 787 (1955); also Phys. Rev., 98, 1787 (1955).

Rei65 F. Reif, Fundermentals of Statistical and Thermal Physics (McGraw-Hill, 1965).

Rhi70 W.-K. Rhim, A. Pines, and J.S. Waugh, Phys. Rev. Lett., 25, 218 (1970); also see Phys. Rev., B3, 684 (1971).

Sch70 A.P. Schuch and R.L. Mills, J. Chem. Phys., 52, 6000 (1970).

Sco59 R.B. Scott, Cryogenic Engineering (D. Van Nostrand Co., Inc., 1959).

Sco76 T.A. Scott, Phys. Rep., 27, 89 (1976).

Sef78 M.D. Sefcik and H.K. Yuen, Thermochim. Acta, 26, 297 (1978).

She63 P.G. Shewmon, Diffusion in Solids (McGraw-Hill, N. Y., 1963).

She69 J.N. Sherwood, Mol. Cryst. Liq. Cryst., 9, 37 (1969).

She79 J.N. Sherwood, editor, The Plastically Crystalline State (John Wiley and Sons, N. Y., 1979).

Sir77 B.E. Sirovich and R.E. Norberg, Phys. Rev., B15, 5107 (1977).

Sli61 C.P. Slichter and W.C. Holton, Phys. Rev., 122, 1701 (1961).

Sli64 C.P. Slichter and D.C. Ailion, Phys. Rev., 135, A1099 (1964).

Sli80 C.P. Slichter, Principles of Magnetic Resonance (Springer-Verlag, N. Y., 1980), 2nd ed..

Sme24 J. de Smedt and W.H. Keesom, Proc. Acad. Sci. Amsterdam, 27, 839 (1924); also Z. Krist., 62, 312 (1926).

Spi74 H.W. Spiess, R. Grosescu, and U. Haeberlen, Chem. Phys., 6, 226 (1974); also see H.W. Spiess, Chem. Phys., 6, 217 (1974).

Spi80 H.W. Spiess, J. Chem. Phys., 72, 6755 (1980).

Ste57 R. Stevenson, J. Chem. Phys., 27, 673 (1957).

Ste69 R. Van Steenwinkel, Z. Naturforsch., A24, 1526 (1969).

Sto66 D.E. Stogryn and A.P. Stogryn, Molec. Phys., 11, 371 (1966).

Str62 W.E. Streib, T.H. Jordan, and W.N. Lipscomb, J. Chem. Phys. 37, 2962 (1962).

Sul82 N.S. Sullivan, D. Estève, and M. Devoret, J. Phys. C, 15, 4895 (1982).

Swe55 C.A. Swenson, J. Chem. Phys., 23, 1963 (1955).

Tol80 A.M. Tolkachev, V.G. Manzhelii, V.P. Azarenkov, A. Ezhovski, and E.A. Koscbutskaya, Sov. J. Low Temp. Phys., 6, 747 (1980).

Tor53 H.C. Torrey, Phys. Rev., 92, 962 (1953).

Van48 J.H. Van Vleck, Phys. Rev., 74, 1168 (1948).

Veg34 L. Vegard, Z. Physik, 88, 235 (1934).

Wol74 D. Wolf, Phys. Rev., B10, 2724 (1974).

Yen63 W.M. Yen and R.E. Norberg, Phys. Rev., 131, 269 (1963).

Yu83 I. Yu, S. Washburn, M. Calkins, and H. Meyer, J. Low Temp. Phys., 51, 401 (1983); also see I. Yu, S. Washburn, and H. Meyer, Solid State Commun., 40, 693 (1981).

VITA

Shang-Bin Liu

Born in Taichung, Taiwan, Republic of China, September 12, 1957. Graduated from Taiwan First Provincial High School in Taichung, May 1975, B.S. in Physics, Chung Yuan University, Taiwan, June 1979. Full-time teaching and research assistant in the Department of Physics, Chung Yuan University, July 1979 - June 1980.

In August 1980, the author entered The College of William and Mary as a graduate student of Physics. Received his M.S. in Physics in May 1982, and continued his doctoral research at William and Mary with a concentration in experimental NMR study of Solid State Physics. While at William and Mary, the author has published six articles in scientific journals and delivered or took part in several Physics meetings.

In August 1985, the author was accepted as a joined post-doctoral research fellow at Lawrence Berkeley Laboratory by the University of California, Berkeley and Stanford University.